

Self-avoiding walks and polygons crossing a domain on the square and hexagonal lattices.

Anthony J Guttmann

School of Mathematics and Statistics, The University of Melbourne, Vic. 3010, Australia

E-mail: guttmann@unimelb.edu.au

ORCID ID: 0000-0003-2209-7192

Iwan Jensen

College of Science and Engineering, Flinders University at Tonsley, GPO Box 2100, Adelaide, SA 5001, Australia

E-mail: iwan.jensen@gmail.com

ORCID ID: 0000-0001-6618-8470

Abstract. We have analysed the recently extended series for the number of self-avoiding walks (SAWs) $C_L(1)$ that cross an $L \times L$ square between diagonally opposed corners. The number of such walks is known to grow as $\lambda_S^{L^2}$. We have made more precise the estimate of λ_S , based on additional series coefficients provided by several authors, and refined analysis techniques. We estimate that $\lambda_S = 1.7445498 \pm 0.0000012$. We have also studied the subdominant behaviour, and conjecture that

$$C_L(1) \sim \lambda_S^{L^2 + bL + c} \cdot L^g,$$

where $b = -0.04354 \pm 0.0001$, $c = 0.5624 \pm 0.0005$, and $g = 0.000 \pm 0.005$.

We implemented a very efficient algorithm for enumerating paths on the square and hexagonal lattices making use of a minimal perfect hash function and in-place memory updating of the arrays for the counts of the number of paths.

Using this algorithm we extended and then analysed series for SAWs spanning the square lattice and self-avoiding polygons (SAPs) crossing the square lattice. These are known to also grow as $\lambda_S^{L^2}$. The sub-dominant term λ^b is found to be the same as for SAWs crossing the square, while the exponent $g = 1.75 \pm 0.01$ for spanning SAWs and $g = -0.500 \pm 0.005$ for SAPs.

We have also studied the analogous problems on the hexagonal lattice, and generated series for a number of geometries. In particular, we study SAWs and SAPs crossing rhomboidal, triangular and square domains on the hexagonal lattice, as well as SAWs spanning a rhombus. We estimate that the analogous growth constant $\lambda_H = 1.38724951 \pm 0.00000005$, so an even more precise estimate than found for the square lattice. We also give estimates of the sub-dominant terms.

PACS: 05.50.+q, 05.10.-a, 02.60.Gf

MSC: 05A15, 30B10, 82B20, 82B27, 82B41

Keywords: Self-avoiding walks, exact enumeration algorithms, power-series expansions, asymptotic series analysis

1. Introduction

A n -step self-avoiding walk (SAW) ω on a regular lattice is a sequence of *distinct* vertices $\omega_0, \omega_1, \dots, \omega_n$ such that each vertex is a nearest neighbour of its predecessor. SAWs are considered distinct up to translations of the starting point ω_0 . If ω_0 and ω_n are nearest-neighbours we can form a closed $(n + 1)$ -step self-avoiding polygon (SAP) by adding an edge between the two end-points.

We consider SAWs on an $L \times L$ square lattice, with the walks starting at the north-west corner $(0, L)$ and finishing at the south-east corner $(L, 0)$, and constrained within the square (see the first diagram in Figure 1). Clearly such walks vary in length from a minimum of $2L$ to a maximum of $L^2 + 2L$ (if L is even). Guttmann and Whittington [1] computed the first 7 terms in 1990, then Bousquet-Mélou, Guttmann and Jensen [2] computed the terms up to $L = 19$. Iwashita et al. [3] computed the next two terms, $L = 20$ and 21 , R. Spaans computed three more terms, $L = 22$ to 24 , and Iwashita [4] computed the terms for $L = 25$ and 26 . Details can be found in the On-line Encyclopaedia of Integer Sequences [5], OEIS [A007764](#). Note that the listing in the OEIS runs from 1 to 27, which in our notation is $L = 0$ to 26 .

Recall that the number of SAWs in the bulk, c_n , grows exponentially with length n as μ^n , where μ depends on the lattice. For the hexagonal lattice it is known [6] that $\mu = \sqrt{2 + \sqrt{2}}$, while for the square lattice the growth constant μ has only been estimated numerically. The most precise estimate $\mu = 2.63815853032790(3)$ was obtained by Jacobsen, Scullard and Guttmann [7].

We will be interested in the generating function $C_L(x) = \sum_{n \geq 2L} c_n x^n$, where c_n denotes the number of SAWs of length n crossing the square from $(0, L)$ to $(L, 0)$. Madras [8] proved that the limits $\mu_1(x) := \lim_{L \rightarrow \infty} C_L(x)^{1/L}$ and $\mu_2(x) := \lim_{L \rightarrow \infty} C_L(x)^{1/L^2}$ are well defined in $\mathbb{R} \cup \{+\infty\}$. More precisely, Madras proved (i) $\mu_1(x)$ is finite for $0 < x < 1/\mu$, and is infinite for $x > 1/\mu$. Moreover, $0 < \mu_1(x) < 1$ for $0 < x < 1/\mu$ and $\mu_1(1/\mu) = 1$. (ii) $\mu_2(x)$ is finite for all $x > 0$. Moreover, $\mu_2(x) = 1$ for $0 < x \leq 1/\mu$ and $\mu_2(x) > 1$ for $x > 1/\mu$.

The existence of the limit

$$\lim_{L \rightarrow \infty} C_L(1)^{1/L^2} = \lambda_S \tag{1}$$

was proved in both [9] and [1] by different methods. In [2] we estimated $\lambda_S = 1.744550 \pm 0.000005$. Using the longer series now available, we have sharpened this to $\lambda_S = 1.7445498 \pm 0.0000012$. We have also estimated the sub-dominant terms by finding precise numerical evidence for the asymptotic behaviour

$$C_L(1) \sim \lambda_S^{L^2 + bL + c} \cdot L^g, \tag{2}$$

where $b = -0.04354 \pm 0.0001$, $c = 0.5624 \pm 0.0005$, and $g = 0.000 \pm 0.005$, from which we conjecture that $g = 0$, exactly.

For SAPs crossing a square we calculated the coefficients up to $L = 26$ and then analysed the data for the first time. The analysis clearly demonstrated that the two problems have the same growth constant. We conjecture that the subdominant term

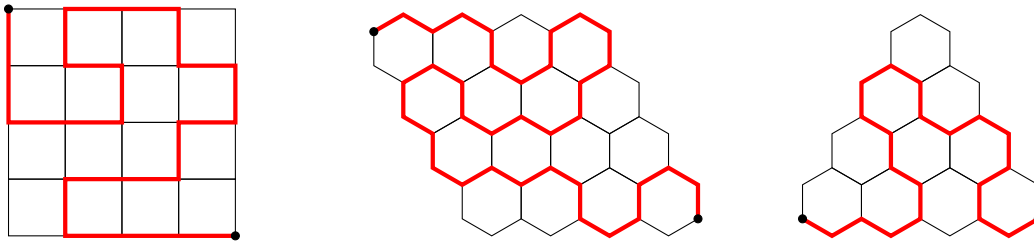


Figure 1: A square domain and rhomboidal and triangular domains of size $n = 4$ on the hexagonal lattice. Walks must extend between the points indicated by black circles as illustrated by the red walks.

λ^b is the same as for crossing SAWs, and that the corresponding exponent $g = -\frac{1}{2}$. For SAWs spanning a square we extended the known series up to $L = 26$. This is a superset of SAWs crossing the square, as the origin can be any vertex on the left boundary and the end-point can be any vertex on the right boundary. In [8] it was proved that the two problems have the same growth constant and this is of course consistent with our analysis. We conjecture that the λ^b term is the same as for crossing SAWs and that $g = \frac{7}{4}$.

We have also studied the analogous problems on the hexagonal lattice. We initially considered the problem on a square domain of the hexagonal lattice (see the last two diagrams in Figure 15), but this was soon found to be a rather unnatural domain, as the paths changed according as the size L of the lattice was odd or even. A more natural domain is a rhombus, shown as the second diagram in Figure 1, or a triangular domain, shown as the third diagram in Figure 1. We studied both self-avoiding walks (SAWs) and self-avoiding polygons (SAPs) in these three domains. For the triangular domain, we studied two cases, according as the path is forced to include the top vertex of the triangle or not. We also studied SAWs which *span* a rhombus of width L .

In Section 2 we give a detailed description of the new and very efficient algorithm we used to calculate the series for SAWs crossing a rhombus and briefly mention how to amend the algorithm to enumerate other problems such as SAPs. In Section 3 we give a brief description of the methods we used in our analysis of the series. Further details can be found in Appendix A and Appendix B. Section 4.1 contains a detailed analysis of the extended series for SAWs crossing a square with SAPs and spanning SAWs given a more cursory treatment. This is followed in Section 4 by the results of our detailed asymptotic analysis of SAWs crossing rhomboidal and triangular domains with several other problems briefly mentioned. Section 6 contains our conclusions and gives a summary of the estimates we have obtained.

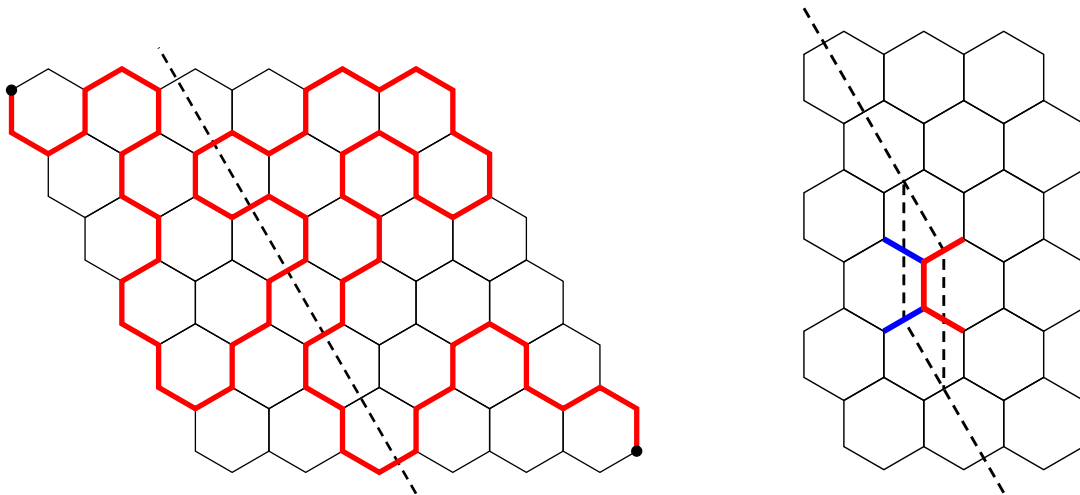


Figure 2: An example (left panel) of a SAW crossing a rhomboidal domain of the hexagonal lattice intersected by a TM line. The basic TM move (right panel) in which the intersection is moved so as to add another two vertices and three edges to the section of the domain already visited. The states of the two blue ‘incoming’ edges determines the type of update to apply while adding the three red edges to the visited section of the domain.

2. Algorithm to enumerate SAWs crossing a rhombus.

The algorithm we use to count the number SAWs on domains of the hexagonal lattice builds on the pioneering work of Enting [10] who enumerated square lattice self-avoiding polygons and extended by Conway, Enting and Guttmann [11] to enumerate square lattice SAWs. An algorithm for the enumeration of hexagonal SAWs was described in [12] and a detailed description of the general method can be found in [13].

2.1. Transfer matrix algorithm

If we take an example of a SAW crossing a rhombus and draw an line across the domain as shown in Figure 2 we observe that the partial SAW to the left of the intersection consists of arcs connecting two edges on the intersection (we shall refer to these as arc-ends), and a single edge that is not connected to any other edge on the intersection (we call this a free end). The free end is connected to the vertex in the upper left corner of the domain and the SAW must terminate in the lower right corner.

We are not allowed to form closed loops, so two arc ends can only be joined if they belong to different arcs. We must also ensure that the graphs we count have just a single component. To exclude arcs which close on themselves we label the occupied edges in such a way that we can easily determine whether or not two ends belong to the same arc. On two-dimensional lattices this can be done by relying on the fact that arcs can never intertwine. Each arc end is assigned a label depending on whether it is the lower

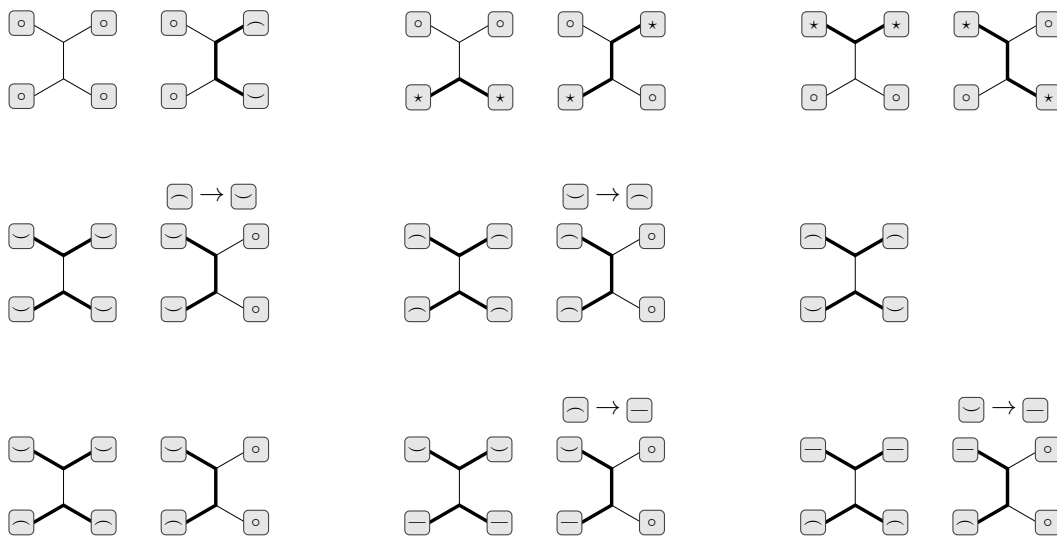


Figure 3: The possible updates in a TM move with thin edges empty and thick edges occupied by the walk. In the top row \star refers to any type of occupied edge \square , $\langle \rangle$, or \rangle . Relabelling of arc ends are indicated above the update, i.e., for the second transition in the second row two lower arc ends are connected and the matching upper end is relabelled as a lower end.

or upper end of an arc and these labels can be viewed as balanced parenthesis. We shall refer to the configuration along the intersection as a *signature*, denoted by Σ , which can be represented by a string of edge states, σ_i , where

$$\sigma_i = \begin{cases} \square & \text{empty edge,} \\ \langle & \text{lower arc end,} \\ \rangle & \text{upper arc end,} \\ \square & \text{free end.} \end{cases} \quad (3)$$

Take the SAW in Figure 2 and consider the configuration associated with the partial SAW to the left of the line. Reading from bottom to top we find the signature $\Sigma = \langle \square \rangle \square \square \square \square \square$. Since all SAWs have to cross the rhombus it readily follows that any signature contains one free edge surrounded by a string of empty states and arc ends on either side (with the arc ends forming balanced parenthesis).

For each signature Σ we simply count the number of partial SAWs, $\mathcal{C}(\Sigma)$. SAWs in a given domain of the hexagonal lattice are counted by moving the intersection so as to add two vertices and three edges at a time, as illustrated in Figure 2. The updating of the counts $\mathcal{C}(\Sigma)$ depends on the states of the edges to the left of the new vertices. In Figure 3 we display the possible local ‘input’ states and the ‘output’ states which arise as the kink in the boundary is propagated by one step. Not all the possible local input states are displayed since some are related by an obvious reflection symmetry with straightforward changes to the corresponding updating rules. We shall refer to the signature before the move as the *source*, Σ_S , and a signature produced as a result of the

move as a *target*, Σ_T . In all cases we see that the first update has the source appearing as a target as well. In the second row, last panel, we cannot connect the arc ends since this would result in the formation of a cycle. Most of the updates are local and involve only the two edges in the kink, but some of the updates involves a non-local transformation of the signature. This happens when we connect two lower (upper) arc ends or a free end to a lower (upper) arc end. In these cases we need to locate a matching arc end in the signature and relabel it accordingly. We illustrate these here:



Two consecutive blue tiles indicate the edges that are involved in the update as per Figure 2, while the isolated blue tile indicate the edge which has a change of state. In the first example we connect two lower arc ends (second row second update of Figure 3) and we then have to relabel the upper arc end of the inner arc to a lower arc end as indicated. How do we find the matching arc end? We start at the update position of the innermost arc and set a counter to 1, we then scan to the right and increase the counter by 1 for every \lfloor we encounter and decrease the counter by 1 for every \rfloor ; once the counter records a value of 0 we have found the matching end. Similarly in the second example (illustrating the last update in row three of Figure 3) we connect an upper arc end to the free end and we then have to locate the matching lower end of the arc and change the state from \lfloor to \lceil .

2.2. Motzkin path representation of signatures

It is possible to represent the signatures as Motzkin paths, which are directed walks from $(0,0)$ to $(n,0)$ in the first quadrant of the square lattice with step-set $\Omega = \{(1,0), (1,1), (1,-1)\}$, see OEIS [A001006](#) for numerous references to this classical combinatorial problem. We shall refer to the steps as horizontal, up and down steps, respectively. The basic mapping from a signature to a Motzkin path is to map \circ to horizontal steps, \lfloor to up steps, and \rfloor to down steps.

What about the free end? Since the walk has to cross the domain the free end can never be enclosed inside an arc and therefore splits the signature into two ‘halves’ such that on either side of the free end one has a standard Motzkin path. Next we consider what happens to updates involving a free end and show that we don’t need to explicitly keep track of the free end but can treat it as if it were an (excess) upper end arc, which we denote \lceil .

$\lceil \circ$: An input of $\lceil \circ$ (or $\circ \lceil$) produces outputs $\circ \lceil$ and $\lceil \circ$ which is the same as for an input $\lceil \circ$ with the free end remaining the excess \lceil .

$\lceil \lfloor$: $\lceil \lfloor \rightarrow \lceil \lfloor$ is clearly the same as $\lceil \lfloor \rightarrow \lceil \lfloor$. In the case $\lceil \lfloor \rightarrow \circ \circ$ we are connecting a free end to a lower arc end and relabelling the matching upper

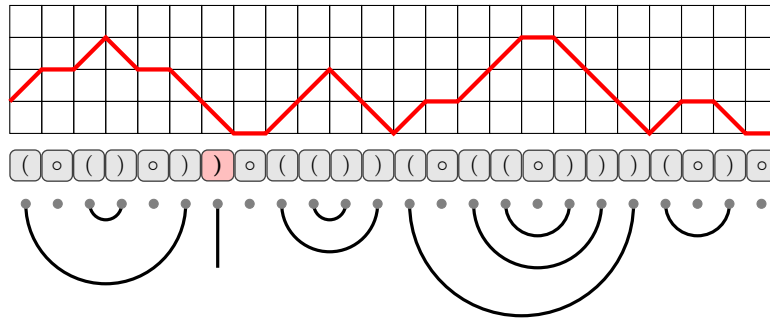


Figure 4: Illustration of the representation of an arc configuration along the TM intersection line (grey circles mark the intersection with an edge), the corresponding signature, and the corresponding Motzkin path starting at $(0,1)$ and ending at $(24,0)$. The free end can be represented by an excess upper arc end $)$ and located as the first return of the Motzkin path to level 0.

end as free. However, this is equivalent to $)\textcircled{)} \rightarrow \textcircled{)}\textcircled{)}$ with the incoming $)$ now moving to the position of the matching $\textcircled{)}$ of the arc with no change of state required.

$\textcircled{)}\textcircled{)} : \textcircled{)}\textcircled{)} \rightarrow \textcircled{)}\textcircled{)}$ is clearly the same as $\textcircled{)}\textcircled{)} \rightarrow \textcircled{)}\textcircled{)}$. In the case $\textcircled{)}\textcircled{)} \rightarrow \textcircled{)}\textcircled{)}$ we are connecting a free end to an upper arc end and relabelling the matching lower end as free. However, this is equivalent to $\textcircled{)}\textcircled{)} \rightarrow \textcircled{)}\textcircled{)}$ with the incoming $)$ now moving to the position of the matching $\textcircled{)}$ of the arc and being relabelled as $\textcircled{)}$.

$\textcircled{)}\textcircled{)} / \textcircled{)}\textcircled{)}$: Not possible since free end would be enclosed inside an arc.

It now follows that the set of signatures can be represented as the set of Motzkin paths starting at height 1, i.e. at vertex $(0,1)$, and ending at $(L+1,0)$. This is another well known combinatorial problem as evidenced by its low sequence number, OEIS [A002026](#). Should we need to know the position of the free end (as it happens we don't for this problem) it is easy to find it as the excess $)$ when looking from the first state in the signature. In Motzkin parlance the position of the free end corresponds to the *first* return of the path to height 0. The representation is illustrated in Figure 4.

2.3. Minimal perfect hashing

We implement the minimal perfect hashing scheme of Iwashita *et al* [4]. Let $\mathcal{M}_{(m,h)}^{(0)}$ be the set of m -step Motzkin paths starting at height 0 and ending at height h . Similarly, let $\mathcal{M}_{(n,h)}^{(1)}$ be the set of n -step Motzkin paths starting a height 1 and ending at height h . The total set of states is $\mathcal{M}_{(L+1,0)}^{(1)}$ since there are $L+1$ edges along the TM intersection. So we seek to construct a mapping $\Phi : \mathcal{M}_{(L+1,0)}^{(1)} \rightarrow \{1, \dots, |\mathcal{M}_{(L+1,0)}^{(1)}|\}$. We implement this as a sum of two functions

$$\Phi(\Sigma) = \Phi_L(\Sigma_L) + \Phi_R(\Sigma_R), \quad (4)$$

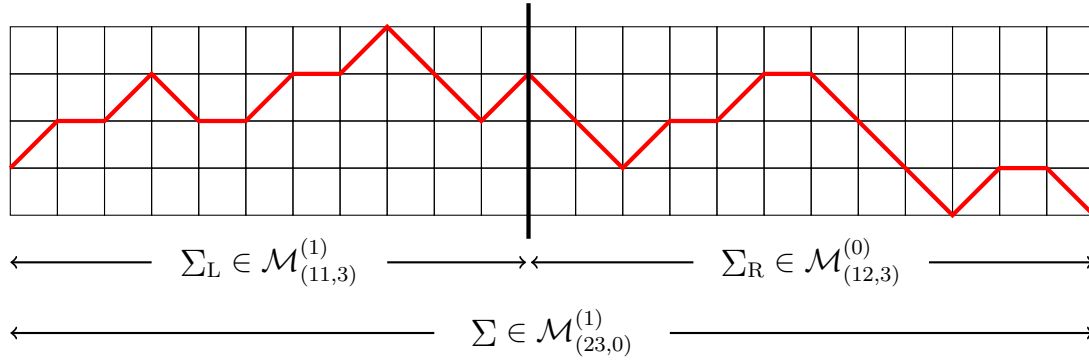


Figure 5: Illustration of the splitting of a Motzkin path representing a signature, $\Sigma \in \mathcal{M}_{(23,0)}^{(1)}$ ($L = 22$), into left and right halves of height $h = 3$, with $\Sigma_L \in \mathcal{M}_{(11,3)}^{(1)}$ and $\Sigma_R \in \mathcal{M}_{(12,3)}^{(0)}$. Note that the right Motzkin path has to be reversed, i.e., it starts at $(23,0)$ and proceeds leftwards to $(11,3)$.

where Σ_L is the left part of the signature and Σ_R the right part. We divide the signature at the halfway point so that Σ_L contains the first $m = \lfloor (L+1)/2 \rfloor$ states of Σ , and Σ_R the remaining $n = L+1 - m$ states. We can view Σ as the concatenation of two Motzkin paths of height h with $0 \leq h \leq m$. We then have that $\Sigma_L \in \mathcal{M}_{(m,h)}^{(1)}$ and $\Sigma_R \in \mathcal{M}_{(n,h)}^{(0)}$, though the Motzkin path from $\mathcal{M}_{(n,h)}^{(0)}$ has to be reversed, see Figure 5.

We divide the storage array for the counts into sections based on the height h of the signatures $\Sigma \in \mathcal{M}_{(L+1,0)}^{(1)}$. Each $\Sigma_L \in \mathcal{M}_{(m,h)}^{(1)}$ can be concatenated with any reversed path from $\mathcal{M}_{(n,h)}^{(0)}$. The total number of paths of height h is therefore $|\mathcal{M}_{(m,h)}^{(1)}| \cdot |\mathcal{M}_{(n,h)}^{(0)}|$, and this is the size of the section of the storage array required to contain the counts for signatures of height h . Each main section of the storage array is divided into subsections of size $|\mathcal{M}_{(n,h)}^{(0)}|$ containing the counts of the signatures with a particular left part Σ_L . The paths in $\mathcal{M}_{(m,h)}^{(1)}$ and $\mathcal{M}_{(n,h)}^{(0)}$ are sorted in lexicographical order (using $\ominus < \odot < \circ$) so that paths can be assigned unique indices I_L and I_R (note there is separate index function for each h and L). Define the number b_h as

$$b_0 := 0,$$

$$b_{h+1} := b_h + |\mathcal{M}_{(m,h)}^{(1)}| \cdot |\mathcal{M}_{(n,h)}^{(0)}|,$$

then we define

$$\Phi_L(\Sigma_L) = b_h + (I_L - 1) \cdot |\mathcal{M}_{(n,h)}^{(0)}|$$

$$\Phi_R(\Sigma_R) = I_R.$$

Φ_L tells us which subsection of the storage array to use and Φ_R gives us the position within a given subsection.

2.4. Data representation and storage

The number of signatures $|\mathcal{M}_{(L+1,0)}^{(1)}|$ can be expressed in terms of Motzkin numbers $M_n = |\mathcal{M}_{(n,0)}^{(0)}|$ (OEIS [A001006](#)) since $|\mathcal{M}_{(L+1,0)}^{(1)}| = M_{L+2} - M_{L+1}$ (OEIS [A002026](#)). The Motzkin numbers are given by the recurrence

$$M_0 = M_1 = 1, \quad (n+2)M_n = (2n+1)M_{n-1} + 3(n-1)M_{n-2} \quad (5)$$

and have the generating function

$$\mathcal{M}(z) = \sum_{n=0} M_n z^n = (1 - z - \sqrt{1 - 2z - 3z^2}) / (2z^2). \quad (6)$$

From this it follows immediately that $|\mathcal{M}_{(L+1,0)}^{(1)}| \sim 3^L$ and this gives the asymptotic growth in the storage required for the counts $\mathcal{C}(\Sigma)$. This growth in storage is the main limitation on the maximum size L_{\max} that we can attain. We therefore perform all calculations of the walk counts modulo several prime numbers p_k which yields remainders of $C_L(1)$ modulo p_k . The exact counts are then obtained from the remainders using the Chinese remainder theorem. We generally use primes of the form $p_k = 2^{62} - r_k$, such that p_k are the largest primes less than 2^{62} . The counts $\mathcal{C}(\Sigma)$ can therefore be stored in an array of 64-bit integers with $\Phi(\Sigma)$ giving the position where $\mathcal{C}(\Sigma)$ is stored.

The signatures are represented as 64-bit integers with 2 bits required for each state, with $\ominus = 00$, $\square = 10$, and $\circlearrowright = 01$. The left and right parts of a signature can then be represented by a 32-bit integer and the hash functions Φ_L and Φ_R can be coded directly as simple arrays or look-up tables. The total size of these two arrays is about 2^{L+2} so insignificant compared to the storage needed for the counts. The integer representation of signatures also means that transformations between a signature Σ and its left and right parts Σ_L, Σ_R and from sources to targets can be done very efficiently using bit-wise manipulations.

2.5. In-place memory updating

By controlling the order in which we access the signatures we can ensure that the counts can be updated in-place without the need for any temporary storage. The way we order the signatures is by height and for given height in lexicographical increasing order. Generally speaking, in-place updating is safe if a signature is updated only after it has been processed. The specific order of processing is controlled by the position at which we divide the signature into two halves. Importantly this dividing position need not be the same as the one used to construct the hash function and can be changed between iterations of the TM algorithm. The updates illustrated in Figure 3 shows that processing a given source signature Σ_S always give rise to the same signature (as a target). A signature mapping to itself results in no change to its count and hence nothing needs to be done and in-place updating is trivially safe. We now consider the updates in detail and show how in-place updating can be done safely.

$\circ\circ$: Processing the signature $\Sigma_S = \Sigma_L\circ\circ\Sigma_R$ leads to Σ_S and the new signature $\Sigma_T = \Sigma_L(\circ\circ)\Sigma_R$. Updating the count for Σ_T is safe since Σ_T does not give rise to any new target signatures (apart from itself) when processed.

$\circ(\circ)/(\circ\circ)$: Processing $\Sigma_1 = \Sigma_L\circ(\circ)\Sigma_R$ leads to Σ_1 and the signature $\Sigma_2 = \Sigma_L(\circ\circ)\Sigma_R$, while similarly processing Σ_2 gives rise to Σ_2 and Σ_1 . In-place updating of the counts for Σ_1 and Σ_2 is safe provided they are updated simultaneously, which is easily achieved.

$\circ\circ)/\circ\circ$: Same as above.

$(\circ\circ)$: Processing the signature $\Sigma_S = \Sigma_L(\circ\circ\circ\circ)\Sigma_R$ leads to Σ_S and the new signature $\Sigma_T = \Sigma_L\circ\circ(\circ\circ)\Sigma_R$. Note that the matching upper arc ends \circ need not be consecutive or next to $(\circ\circ)$. We now look at the four sites involved in the update and consider how the height of the signature at the dividing position changes. We have

$$\begin{array}{cccccc|cccc} (\circ & | & (\circ & | & \circ & | & \circ & | & \circ \\ 0 & & 1 & & 2 & & 1 & & 0 \end{array} \rightarrow \begin{array}{cccc|cccc} \circ & | & \circ & | & (\circ & | & \circ \\ 0 & & 0 & & 0 & & 1 & & 0 \end{array}$$

The possible dividing positions are indicated by vertical lines and the numbers below indicate the additional height of the signature from the height of Σ_L .

We see that Σ_T is never higher than Σ_S and when they have the same height Σ_T is lexicographically smaller than Σ_S . Hence in all cases we process Σ_T before updating its count and in-place updating is therefore safe.

$\circ\circ)$: Processing $\Sigma_S = \Sigma_L(\circ\circ\circ\circ)\Sigma_R$ leads to Σ_S and $\Sigma_T = \Sigma_L(\circ\circ)\circ\circ\Sigma_R$. We have

$$\begin{array}{cccccc|cccc} (\circ & | & (\circ & | & \circ & | & \circ \\ 0 & & 1 & & 2 & & 1 & & 0 \end{array} \rightarrow \begin{array}{cccc|cccc} (\circ & | & \circ & | & \circ & | & \circ \\ 0 & & 1 & & 0 & & 0 & & 0 \end{array}$$

As for the case above in-place updating is safe.

$(\circ\circ)$: No new signatures.

$\circ(\circ)$: Processing $\Sigma_S = \Sigma_L\circ(\circ)\Sigma_R$ leads to Σ_S and $\Sigma_T = \Sigma_L\circ\circ\Sigma_R$. We have

$$\begin{array}{cc|cc} \circ & | & (\circ & | \\ 0 & & -1 & & 0 \end{array} \rightarrow \begin{array}{cc|cc} \circ & | & \circ & | \\ 0 & & 0 & & 0 \end{array}$$

In-place updating is safe when the additional height is 0. There is a problem when the dividing position splits the signature between \circ and $(\circ$. In that case Σ_T is higher than Σ_S and in-place updating is unsafe since the count of Σ_T is updated before Σ_T is processed.

The upshot of the above considerations is that in-place updating can be safely done provided the dividing position never splits the signature between two edges involved in an update. Thankfully we can easily avoid this from happening since we can change the dividing position so as to avoid such splits.

Algorithm 1 Calculate the number of SAWs crossing a rhombus of size L

```

1:  $l_h \leftarrow \lfloor (L+1)/2 \rfloor$ 
2:  $\Phi \leftarrow \text{CONSTRUCTHASHFUNCTION}(l_h)$ 
3:  $l_t \leftarrow l_h - 1$  ▷ Upper signature divider
4:  $l_b \leftarrow l_t - 1$  ▷ Lower signature divider
5:  $\mathcal{C}[k] \leftarrow 0$  for all  $1 \leq k \leq |\mathcal{M}_{(L+1,0)}^{(1)}|$ 
6:  $\mathcal{C}[\Phi(\textcircled{\square}\textcircled{\square} \cdots \textcircled{\square}\textcircled{\square})] \leftarrow 1$ 
7: for  $Row = 0$  to  $L$  do ▷ Build domain column-by-column
8:    $m_h \leftarrow \min(l_t + 1, L + 1 - l_t)$  ▷ Max possible height
9:    $\{\mathcal{M}_{(l_t,h)}^{(1)}, \mathcal{M}_{(L+1-l_t,h)}^{(0)}\} \leftarrow \text{CONSTRUCTSIGNATURES}(l_t)$  ▷  $0 \leq h \leq m_h$ 
10:  for  $Col = L - 1$  to  $l_t$  by  $-1$  do ▷ Build top half of column
11:    for  $h=0$  to  $m_h$  do ▷ Height of signatures
12:      for all  $\Sigma_L \in \mathcal{M}_{(l_t,h)}^{(1)}$  do ▷ Left signatures
13:        for all  $\Sigma_R \in \mathcal{M}_{(L+1-l_t,h)}^{(0)}$  do ▷ Right signatures
14:           $\Sigma_S \leftarrow \Sigma_L \Sigma_R$  ▷ Source signature
15:           $\text{UPDATECOUNTS}(\Sigma_S)$  ▷ Process source signature
16:        end for
17:      end for
18:    end for
19:  end for
20:   $m_h \leftarrow \min(l_b + 1, L + 1 - l_b)$  ▷ Max possible height
21:   $\{\mathcal{M}_{(l_b,h)}^{(1)}, \mathcal{M}_{(L+1-l_b,h)}^{(0)}\} \leftarrow \text{CONSTRUCTSIGNATURES}(l_b)$ 
22:   $Col \leftarrow l_t - 1$  ▷ Add unit cell to column
23:  for  $h=0$  to  $m_h$  do ▷ Height of signatures
24:    for all  $\Sigma_L \in \mathcal{M}_{(l_b,h)}^{(1)}$  do ▷ Left signatures
25:      for all  $\Sigma_R \in \mathcal{M}_{(L+1-l_b,h)}^{(0)}$  do ▷ Right signatures
26:         $\Sigma_S \leftarrow \Sigma_L \Sigma_R$  ▷ Source signature
27:         $\text{UPDATECOUNTS}(\Sigma_S)$  ▷ Process source signature
28:      end for
29:    end for
30:  end for
31:   $m_h \leftarrow \min(l_t + 1, L + 1 - l_t)$  ▷ Max possible height
32:   $\{\mathcal{M}_{(l_t,h)}^{(1)}, \mathcal{M}_{(L+1-l_t,h)}^{(0)}\} \leftarrow \text{CONSTRUCTSIGNATURES}(l_t)$ 
33:  for  $Col = l_t - 2$  to  $0$  by  $-1$  do ▷ Build bottom half of column
34:     $\vdots$  ▷ Repeat lines 11:–18:
35:  end for
36: end for
37: return  $\mathcal{C}[\Phi(\textcircled{\square}\textcircled{\square} \cdots \textcircled{\square}\textcircled{\square})]$ 

```

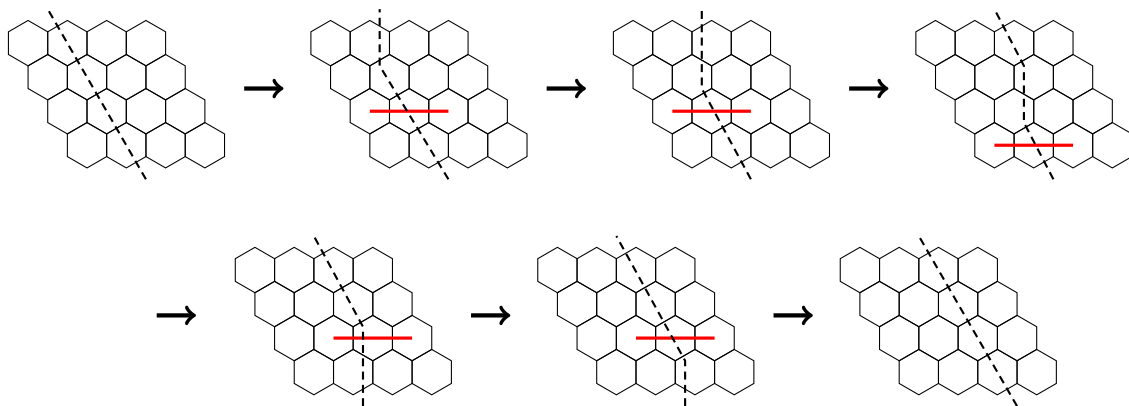


Figure 6: The TM moves used to add an extra column to a rhomboidal domain. The thick red line shows the dividing position during an update.

We are now ready to present our algorithm for counting SAWs crossing a rhombus. Algorithm 1 presents pseudo code for the main body of our algorithm. First up we divide signatures into two halves at position l_h and calculate the corresponding hash function Φ or more specifically the two functions (look-up tables) Φ_L and Φ_R . The hash function Φ remains fixed throughout the entire calculation. The value of l_h determines *where* counts are stored in memory. Then we define two parameters l_t and l_b which determine the *order in which signatures are processed*. Next we initialise the counts to zero except for the signature with a free end at the top vertex. After this comes the main body of the algorithm where we build the rhombus column-by-column up to size L with each column built cell-by-cell as illustrated in Figure 6. Note that the first move, from panel 1 to 2, and the final move are ‘virtual’. These TM intersection moves add just a single edge and this means that all sources and targets are identical and hence no updating is actually required. These moves are included for illustrative purposes only.

We choose the parameters l_t and $l_b < l_h$, because memory access is crucial to the performance of the algorithm and we found that for L large these choices resulted in the best performance. The reason for breaking the column construction into three separate pieces is to allow in-place updating of the counts. During the first loop (at line 10) the position of the divider l_t is below the local states being changed by an update (see Figure 6) so in-place updating can be done safely. Next we change the divider to be at $l_b = l_t - 1$, since otherwise the divider would lie between the two local states in the TM kink and as explained above this would not be safe. We then change back to a divider at l_t (which now lies above the local states of the update) and complete the column. Note that we could have set $l_b = l_t + 1 = l_h$ and completed the column with this divider, but as already stated using dividers strictly less than l_h is faster and the time taken by an extra call to `CONSTRUCTSIGNATURES` is insignificant. The routine `CONSTRUCTSIGNATURES` generates the sets of left and right signatures using a simple back-tracking algorithm.

The updating rules for the counts of the signatures are given in Algorithm 2.

Algorithm 2 Update the counts of signatures

```

1: procedure UPDATECOUNTS( $\Sigma_S$ )
2:    $S \leftarrow \text{INPUTSTATE}(\Sigma_S)$  ▷ States of update edges
3:   if  $S = \begin{smallmatrix} \circ & \circ \end{smallmatrix}$  then
4:      $\Sigma_T \leftarrow \text{CHANGESIGNATURE}(\Sigma_S, \begin{smallmatrix} ( & ) \end{smallmatrix})$  ▷ Insert new arc
5:      $\mathcal{C}[\Phi(\Sigma_T)] \leftarrow \mathcal{C}[\Phi(\Sigma_T)] + \mathcal{C}[\Phi(\Sigma_S)]$  ▷ Update count of target
6:   else if  $S = \begin{smallmatrix} ( & \circ \end{smallmatrix}$  then
7:      $\Sigma_T \leftarrow \text{CHANGESIGNATURE}(\Sigma_S, \begin{smallmatrix} \circ & ( \end{smallmatrix})$ 
8:      $\mathcal{C}[\Phi(\Sigma_T)] \leftarrow \mathcal{C}[\Phi(\Sigma_T)] + \mathcal{C}[\Phi(\Sigma_S)]$  ▷ Update count of target
9:      $\mathcal{C}[\Phi(\Sigma_S)] \leftarrow \mathcal{C}[\Phi(\Sigma_T)]$  ▷ Simultaneous update of source
10:  else if  $S = \begin{smallmatrix} \circ & ( \end{smallmatrix}$  then
11:    NULL ▷ Do nothing. Processed in previous update
12:  else if  $S = \begin{smallmatrix} ) & \circ \end{smallmatrix}$  then
13:     $\Sigma_T \leftarrow \text{CHANGESIGNATURE}(\Sigma_S, \begin{smallmatrix} \circ & ) \end{smallmatrix})$ 
14:     $\mathcal{C}[\Phi(\Sigma_T)] \leftarrow \mathcal{C}[\Phi(\Sigma_T)] + \mathcal{C}[\Phi(\Sigma_S)]$  ▷ Update count of target
15:     $\mathcal{C}[\Phi(\Sigma_S)] \leftarrow \mathcal{C}[\Phi(\Sigma_T)]$  ▷ Simultaneous update of source
16:  else if  $S = \begin{smallmatrix} \circ & ) \end{smallmatrix}$  then
17:    NULL ▷ Do nothing. Processed in previous update
18:  else if  $S = \begin{smallmatrix} ( & ( \end{smallmatrix}$  then
19:     $\Sigma_T \leftarrow \text{RELABELSIGNATURE}(\Sigma_S, \begin{smallmatrix} \circ & \circ \end{smallmatrix}, \begin{smallmatrix} ( \end{smallmatrix})$  ▷ Connect arc ends and relabel
20:     $\mathcal{C}[\Phi(\Sigma_T)] \leftarrow \mathcal{C}[\Phi(\Sigma_T)] + \mathcal{C}[\Phi(\Sigma_S)]$ 
21:  else if  $S = \begin{smallmatrix} ( & ) \end{smallmatrix}$  then
22:    NULL ▷ Do nothing. No new signatures
23:  else if  $S = \begin{smallmatrix} ) & ( \end{smallmatrix}$  then
24:     $\Sigma_T \leftarrow \text{CHANGESIGNATURE}(\Sigma_S, \begin{smallmatrix} \circ & \circ \end{smallmatrix})$  ▷ Connect arc ends
25:     $\mathcal{C}[\Phi(\Sigma_T)] \leftarrow \mathcal{C}[\Phi(\Sigma_T)] + \mathcal{C}[\Phi(\Sigma_S)]$ 
26:  else if  $S = \begin{smallmatrix} ) & ) \end{smallmatrix}$  then
27:     $\Sigma_T \leftarrow \text{RELABELSIGNATURE}(\Sigma_S, \begin{smallmatrix} \circ & \circ \end{smallmatrix}, \begin{smallmatrix} ) \end{smallmatrix})$  ▷ Connect arc ends and relabel
28:     $\mathcal{C}[\Phi(\Sigma_T)] \leftarrow \mathcal{C}[\Phi(\Sigma_T)] + \mathcal{C}[\Phi(\Sigma_S)]$ 
29:  end if
30: end procedure

```

INPUTSTATE simply extracts the states of the two input edges involved in the update. CHANGESIGNATURE changes the states of the input edges to those indicated by the two blue tiles. RELABELSIGNATURE changes the input states to empty states and finds and relabels the matching arc end in those updates where two arc ends are connected in a TM update.

2.6. Parallelisation

The transfer-matrix algorithm is very well suited to parallel computation. In previous work we implemented algorithms using the message passing interface (MPI) [14, 13]

suited for distributed memory systems. For this work we used shared memory computers and hence implemented the parallel algorithms using OpenMP which is somewhat simpler but relies on the same basic ideas. One of the main ways of achieving a good parallel algorithm using data decomposition is to try to find an invariant under the operation of the updating rules. That is we seek to find some property of the signature which does not alter in a single iteration. There is such an invariant since any edge not directly involved in the update cannot change from being empty to being occupied and vice versa (it may change, say, from state \square to \square). That is only the kink edges can change their occupation status. This invariant allows us to parallelise the algorithm in such a way that we can do the calculation completely independently on each core. With the intersection straight (having no kinks) we distribute the data across cores so that signatures with the same occupation pattern along the *lower* half of the intersection are processed by the same core. We then do the TM updates inserting the top-half of a new column. This can be done *independently* by each core because the occupation pattern in the lower half remains unchanged. When reaching the half-way point we redistribute the data so that configurations with the same occupation pattern along the *upper* half of the intersection are processed by the same core and we then do the TM update inserting the bottom-half of a new column. This is then repeated column by column.

2.7. Changes needed to enumerate other hexagonal problems

The changes required to enumerate other types of configurations are mostly straightforward. To enumerate spanning SAWs we just need to change lines 6 and 37 in Algorithm 1. At 6 we need to initialise all signatures with just a single free end in some position (all other states empty) to have a count of one. This means a SAW can start in any position on the left side of the rhombus. Similarly at 37 we need to return the sum of the counts for signatures with just a single free end.

To enumerate SAPs crossing a rhombus the main change to note is that we no longer have a free end and any signature can therefore be represented by a standard Motzkin path from $(0, 0)$ to $(L + 1, 0)$. So the total set of signatures for this problem is $\mathcal{M}_{(L+1,0)}^{(0)}$. Furthermore, we have that $\Sigma_L \in \mathcal{M}_{(m,h)}^{(0)}$ and $\Sigma_R \in \mathcal{M}_{(n,h)}^{(0)}$. Again we need to change lines 6 and 37 of Algorithm 1. Line 6 is changed to: $\mathcal{C}[\Phi(\square \square \cdots \square \square)] \leftarrow 1$. Line 37 is changed to: **return** $\mathcal{C}[\Phi(\square \square \cdots \square \square)]$.

Enumerations in a triangular domain just requires us to change the way in which the transfer matrix intersection is moved, that is, the moves for the rhombus TM calculation shown in Figure 6 have to be changed appropriately.

2.8. Algorithm to enumerate square lattice problems

The algorithm for enumerating walks crossing a square has been described in [4], and for this work we implemented our own version which we won't describe here other than to say that the main body is identical to Algorithm 1, but of course the updating rules

are different, and Algorithm 2 must be amended accordingly. The interested reader can check out the actual code at our GitHub repository (see Section 7).

3. Series analysis

The method of series analysis has, for many years, been a powerful tool in the study of a variety of problems in statistical mechanics, combinatorics, and other fields. In essence, the problem is the following: Given the first N coefficients of the series expansion of some function, (where N is typically as low as 5 or 6, or as high as 100,000 or more), determine the asymptotic form of the coefficients, subject to some underlying assumptions, or equivalently the nature of the singularity of the function.

A typical example is the generating function of self-avoiding walks (SAWs) in dimension two or three. This is believed to behave as

$$F(z) = \sum_n c_n z^n \sim C \cdot (1 - z/z_c)^{-\gamma}. \quad (7)$$

In this case, among regular two-dimensional lattices, the value of z_c is only known for the hexagonal lattice [6], while $\gamma = 43/32$ [15] is believed to be the correct exponent value for all two-dimensional lattices, but this has not been proved.

The method of series analysis is used when one or more of the critical parameters is not known. For example, for the three-dimensional version of the above problems, none of the quantities C , z_c or γ are known exactly. From the binomial theorem it follows from (7) that

$$c_n \sim \frac{C}{\Gamma(\gamma)} \cdot z_c^{-n} \cdot n^{\gamma-1}, \quad (8)$$

where $a_n \sim b_n$ means that $\lim_{n \rightarrow \infty} a_n/b_n = 1$. Here C , z_c , and γ are referred to as the critical amplitude, the critical point (usually the radius of convergence) and the critical exponent, respectively. In combinatorics one often refers to the *growth constant* $\mu = 1/z_c$, as the coefficients are dominated by the term μ^n .

Obtaining these coefficients is typically a problem of exponential complexity, as is the case with our algorithm, described in Section 2. The consequence is that usually fewer than 50 terms are known (and in some cases far fewer).

The standard methods of series analysis include the ratio method, described in Appendix A, and the method of differential approximants, described in Appendix B. A relatively recent development has been the method of series extension [16], described in Appendix C, in which differential approximants based on the exactly known terms is used to obtain a significant number of additional *approximate* terms. These approximate terms, if of sufficient accuracy, can then be used in the ratio method and its extensions to obtain more precise estimates of the various critical parameters.

In our analysis below we make use of all of these methods, but will just refer to them under the assumption that the material in the appendices has been understood.

3.1. Methods of analysis

The existence of the limit (1) and the more detailed asymptotic form (2), which we shall take for granted and provide overwhelming numerical support for, suggests several methods of analysis that one can apply in order to estimate the growth constant λ . For the first method (M1), we look at the quantity

$$\lambda_L := C_L(1)^{1/L^2} \sim \lambda. \quad (9)$$

While it has not been proved that the ratios $R_L := C_L(1)/C_{L-1}(1) \sim \lambda^{2L}$, it is almost certainly true, and we will assume it to be so in our analysis. Given the expectation that $R_L \sim \lambda^{2L}$, for the second method (M2) we define the ratio-of-ratios

$$\mathcal{C}_L := \frac{R_{L+1}}{R_L} = \frac{C_{L+1}(1)C_{L-1}(1)}{C_L(1)^2}. \quad (10)$$

From (2) it follows that

$$\mathcal{C}_L = \lambda^2 \left(1 - \frac{g}{L^2} + O(L^{-3}) \right). \quad (11)$$

All of the sequences defined above will be analysed using ratio methods.

Next we briefly describe three different methods that we have used to estimate the parameters b , c and g in the assumed asymptotic form (2). In the first method (P1) we use our best estimate of λ and form the sequence

$$d_L := C_L(1)/\lambda^{L^2} \sim \lambda^{bL+c} \cdot L^g. \quad (12)$$

This sequence, provided the assumed asymptotic form is correct, behaves as a typical power-law singularity, in which the coefficients grow as $a_n \sim C \cdot \alpha^n \cdot n^g$, and can be analysed as such. With that notation, the growth constant $\alpha = \lambda^b$, and the amplitude $C = \lambda^c$. Of course, we have to use our estimated value of λ .

For the second method (P2) we fit to the assumed form by writing

$$\log d_L \sim b \log(\lambda)L + c \log(\lambda) + g \log L. \quad (13)$$

We then use successive triples of data points $(\log d_{k-1}, \log d_k, \log d_{k+1})$, with $k = 2, 3, \dots, L_{\max} - 1$, to obtain estimates of the parameters $b \log \lambda$, $c \log \lambda$, and g .

The third method (P3) makes use of the ratio \mathcal{C}_L (10). According to its asymptotic form (11), we can fit the sequence $\{\mathcal{C}_L\}$ to $c_0 + c_2/L^2 + c_3/L^3$, so that c_0 should give estimators of λ^2 , and c_2 give estimators of $-g\lambda^2$.

If $C_L(1) \sim \lambda^{L^2}$, then the ratios $R_L = C_L(1)/C_{L-1}(1) \sim \lambda^{2L-1}$, so the exponent γ in the canonical form (8) equals 1. It follows that the corresponding function, $\mathcal{R}(z) := \sum_L R_L z^L$, will have a simple pole at the critical point $z_c = 1/\lambda^2$. If we include sub-dominant terms, so that $C_L(1) \sim \lambda^{L^2+bL+c} L^g$, then $R_L \sim \lambda^{2L-1+b}(1 + O(1/L))$, and all that has changed is the amplitude. The singularity is still a simple pole at $z_c = 1/\lambda^2$. The series $\mathcal{R}(z)$ can therefore be analysed using differential approximants to obtain an estimate for λ .

Since $\mathcal{R}(z)$ has a simple pole this suggests two other ways to estimate λ . Firstly, one can simply form Padé approximants, that is set $P_{m,n}(z) := P_m(z)/Q_n(z)$, where

$P_m(z)$ and $Q_n(z)$ are polynomials of degree m and n , respectively, chosen so the first $n + m + 1$ terms in the Taylor expansion of $P_{m,n}(z)$ coincide with those of $\mathcal{R}(z)$. The first real zero of $Q_n(z)$ will then provide an estimate of $1/\lambda^2$.

The second method is a little more speculative and novel and we are not entirely sure of its validity. We force the differential approximants to have a singularity at a critical point \hat{z}_c close to the expected true value $z_c = 1/\lambda^2$. This is done by forming *biased* differential approximants as outlined in Appendix B.1 and the associated critical exponent is calculated. Many biased differential approximants are formed for each value of the biasing critical point \hat{z}_c and the average critical exponent calculated. One can then conjecture that the value of \hat{z}_c for which the average critical exponent attains the value -1 provides a reasonable estimate for $1/\lambda^2$.

4. Walks and polygons in a square.

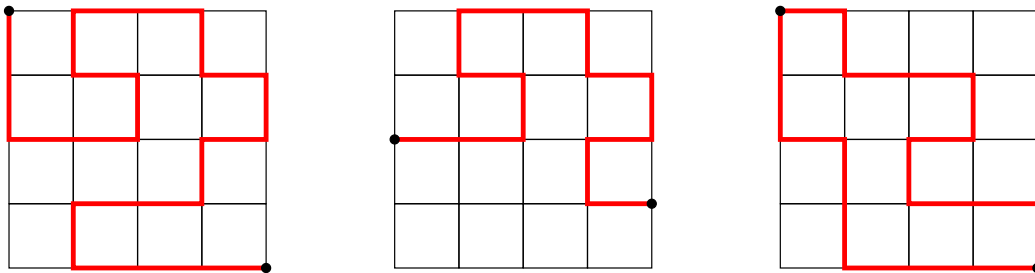


Figure 7: Classes of walk and polygon configurations investigated on the square lattice.

In this section we analyse walks and polygons crossing a square domain of the square lattice, using the techniques just discussed. We study three different variants of the problem, namely SAWs crossing or spanning a square and SAPs crossing a square. These are shown in Figure 7.

4.1. Walks crossing a square

Firstly, we apply method M1 (9) to the analysis of the series for walks crossing a square. For want of greater knowledge about the sub-dominant asymptotic terms we simply extrapolate λ_L against $1/L$. Recall that we only have 27 terms. We therefore use the method of series extension, mentioned above and described in Appendix C, to extend the sequence of *ratios* $R_L = C_L(1)/C_{L-1}(1)$, and this sequence is then used to extend the $C_L(1)$ series. In this way we obtained 20 additional *approximate* coefficients. These are given in Table 1.

We show a plot of λ_L against $1/L$ in the top-left panel of Figure 8, and it is seen to be quite well converged, and can visually be extrapolated to $\lambda_S \approx 1.7442$. It is reasonable to assume that the curvature is due to the presence of higher-order terms, such as $1/L^2$, $1/L^3$ etc. In the top-right panel of Figure 8 we show values of the estimator of

L	$C_L(1)$ estimates.
27	$1.092762277820988255238897693624593273299 \times 10^{176}$
28	$2.092263800732296637339584460940199207179 \times 10^{189}$
29	$1.219188494943327773136239385657818116903 \times 10^{203}$
30	$2.162167627691293760665426155350775028513 \times 10^{217}$
31	$1.167003905184619653378731561256980927898 \times 10^{232}$
32	$1.916990667670442255801047617746147903033 \times 10^{247}$
33	$9.583688332141159129759056552823132225046 \times 10^{262}$
34	$1.458178102419213554003374021702217439866 \times 10^{279}$
35	$6.752333021793147034314988105916341545574 \times 10^{295}$
36	$9.516180772478135635389490590804240161152 \times 10^{312}$
37	$4.081663288146408412423849764027291063947 \times 10^{330}$
38	$5.328162506991801337436456805173755617688 \times 10^{348}$
39	$2.116818597440340726855200831821163701531 \times 10^{367}$
40	$2.559504109272639104369198989850180317538 \times 10^{386}$
41	$9.418767710224918432123841878087214586086 \times 10^{405}$
42	$1.054869066038373202559187284758968442477 \times 10^{426}$
43	$3.595581533556538000636173781717640795638 \times 10^{446}$
44	$3.729975451051537109220327069642553666508 \times 10^{467}$
45	$1.177630435162076031609822304850879989404 \times 10^{489}$
46	$1.131562339582151957192359485190854061339 \times 10^{511}$

Table 1: Estimated coefficients $C_L(1)$.

λ_S assuming λ_L converges to λ_S with correction term $c_1/L + c_2/L^2$, plotted against $1/L^3$, and we estimate $\lambda_S \approx 1.74455$. There is still considerable curvature in this plot and we therefore tried plotting against $1/L^4$ instead, as shown in the bottom-left panel of Figure 8, and in this case the plot appears linear. The straight line is a simple linear fit to the data which intercepts the y -axis at $\lambda_L = 1.74550025$ and we therefore conclude that $\lambda_S \approx 1.744550$. This analysis indicates that the $1/L^3$ correction term is absent or at least has a very small amplitude. Finally in the bottom-right panel of Figure 8 we plot the estimator of λ_S assuming λ_L converges with correction terms $c_1/L + c_2/L^2 + c_4/L^4$, plotted against $1/L^6$. For this plot we have used only the first 4 of the 20 extra approximate coefficients, as using more than this produces some ripples in the plot, indicating that the approximate coefficients are insufficiently precise for such an extreme extrapolation. The linear fit has an intercept at $\lambda_L = 1.745549827$ and hence we estimate $\lambda_S \approx 1.7445498$.

Next, we apply method M2 (10) to the analysis of $C_L(1)$. We show a plot of the ratios $C_L \sim \lambda_L^2$ against $1/L^2$ in the top-left panel of Figure 9. It is seen to display considerable curvature, but can be visually extrapolated to $\lambda_S^2 \approx 3.04345$. In fact the curvature in the plot is suggestive of quadratic behaviour which would mean that C_L depends on $1/L^4$. A plot of C_L against $1/L^4$ is shown in the top-right panel of Figure 9

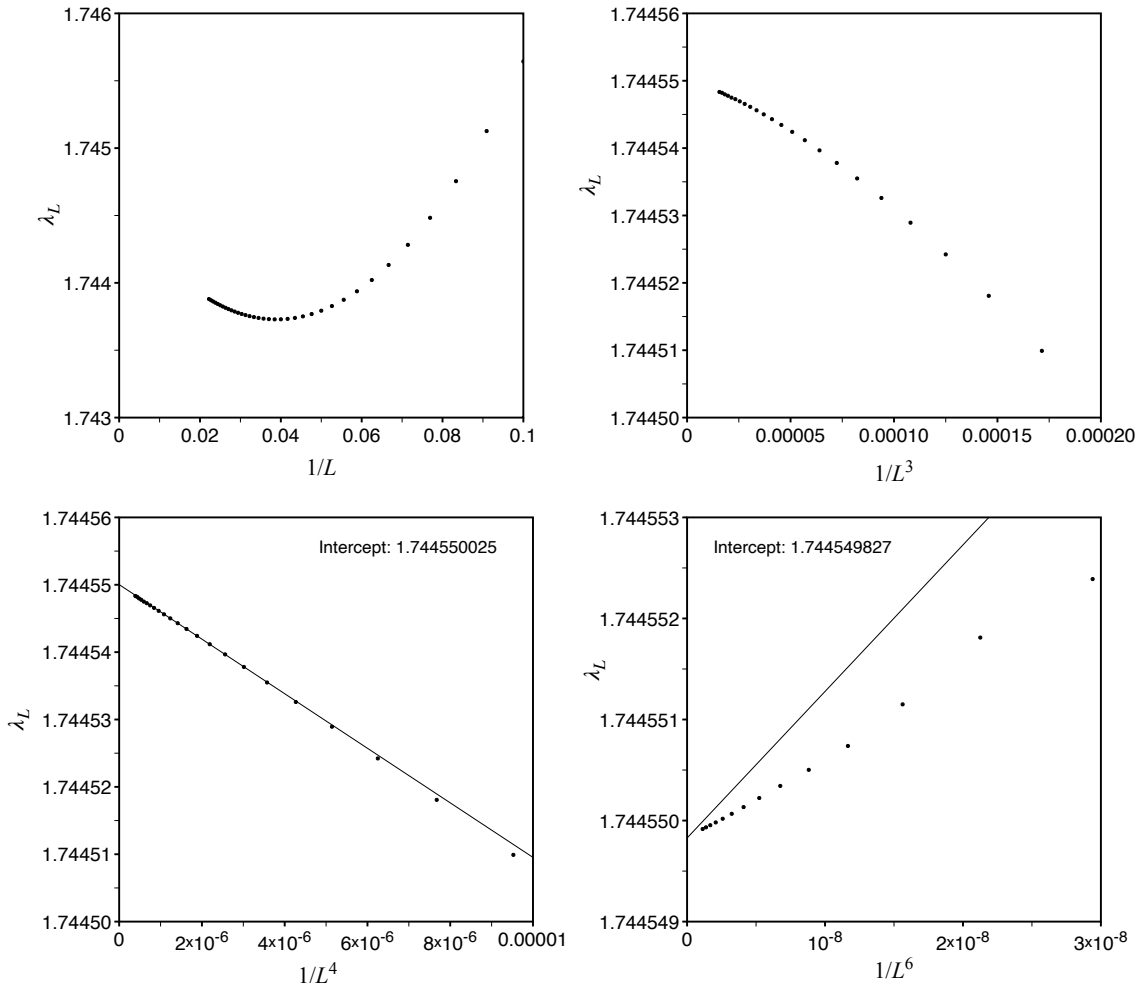


Figure 8: The first panel shows λ_L plotted against $1/L$. The second and third panels show plots of the estimator λ_L using a quadratic correction term against $1/L^3$ and $1/L^4$, respectively. The fourth panel is a plot of the estimator λ_L using the correction term $c_1/L + c_2/L^2 + c_4/L^4$.

and we do indeed see a nice linear plot. The linear fit has intercept at $\lambda_L^2 = 3.043455344$ from which we estimate that $\lambda_S \approx 1.744550$. As above, we now directly include powers of $1/L$ in the extrapolation. In the bottom-left panel of Figure 9 we show the estimator of λ_S^2 assuming λ_L^2 converges with correction term c_4/L^4 , plotted against $1/L^6$ (intercept at 3.043454383). Then in the bottom-right panel of Figure 9 we show the estimator of λ_S^2 assuming λ_L^2 converges with correction terms $c_2/L^2 + c_4/L^4$, plotted against $1/L^6$ (intercept at 3.043454164). For these plot we have used only the first 4 approximate coefficients, for similar reasons to those given above. The two extrapolated values of λ_L^2 are in excellent agreement and we obtain the precise estimate $\lambda_S \approx 1.74454985$. The clear indication from this analysis is that the parameter $g = 0$. To further examine this point we plot in the last panel of Figure 11 the values of $c_2 \sim -g\lambda_L^2$ from the analysis with correction terms $c_2/L^2 + c_4/L^4$. Clearly the value of this parameter is very small and entirely consistent with $g = 0$.

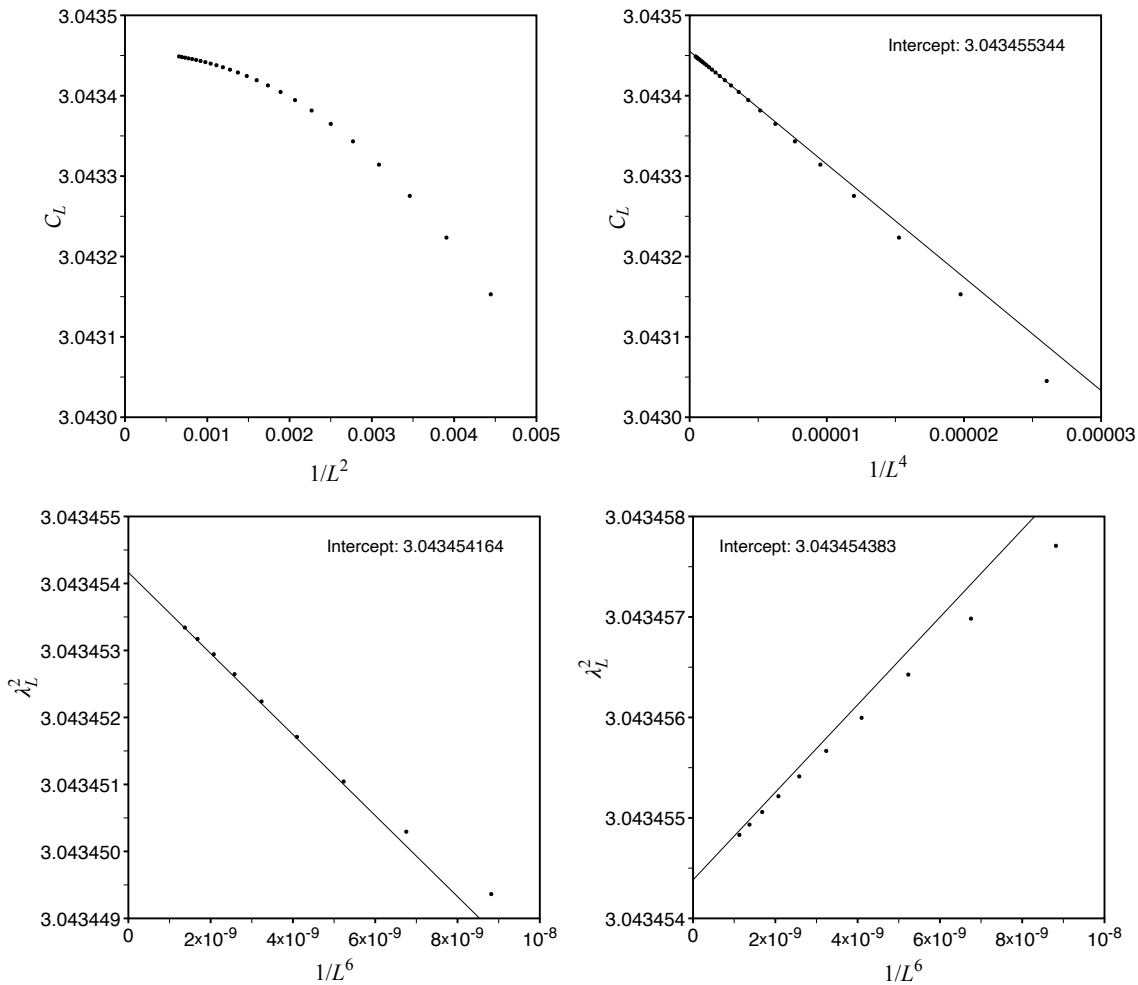


Figure 9: The top two panels show plots of C_L plotted against $1/L^2$ and $1/L^4$, respectively. The bottom panels show plots of the estimators λ_L^2 assuming correction terms c_4/L^4 (left panel) and $c_2/L^2 + c_4/L^4$ (right panel).

Next we will attempt to estimate the parameters b , c and g in the assumed asymptotic form (2) by the methods described in Section 3.1. Using our best estimate of $\lambda_S = 1.7445498$, we first form the sequence $d_L = C_L(1)/\lambda_S^{L^2}$. Usually, ratios are plotted against $1/L$, and the gradient of the linear plot gives a measure of the exponent g . The ratio plot displays considerable curvature when plotted against $1/L$, becoming approximately linear only when plotted against $1/L^3$ as shown in the in the top-left panel of Figure 10. This suggests that the coefficient of $1/L$ in the asymptotic expansion of the expression for the ratios is zero, or at least very small, that is $g \approx 0$. We estimate from this plot that $\alpha = 0.97605 \pm 0.00001$, so that $b = \log \alpha / \log \lambda_S = -0.04355 \pm 0.00001$. From the plot it is clear that there is some residual curvature.

Next we performed a least-squares fit of the data to the form $c_0 + c_3/L^3 + c_4/L^4 + c_5/L^5$ using the data-points from $L = 20$ up to $L = 35$ (we display the data from $L = 15$ to 41) and the resulting plot is shown in the top-right panel. We estimate from this plot that $\alpha = 0.976061 \pm 0.000005$, so that $b = \log \alpha / \log \lambda_S = -0.04354 \pm 0.00001$. Finally,

we use this latter value of α to estimate the value of the parameter c , or equivalently, the amplitude C , by observing that $d_L/\lambda_S^{bL} \sim \lambda_S^c \cdot L^g$. We have argued that $g \approx 0$, so that $d_L/\lambda_S^{bL} \sim \lambda_S^c$. In the bottom-left panel of Figure 10 we show a plot of the estimator of $C = \lambda_S^c$ plotted against $1/L^2$, from which we estimate $C = \lambda_S^c = 1.3673 \pm 0.001$, or $c = 0.5622 \pm 0.0005$. As before we next did a least-squares fit of the data, but now to the form $c_0 + c_2/L^2 + c_3/L^3 + c_4/L^4$, which we display in the bottom-right panel. We estimate $C = \lambda_S^c = 1.36723 \pm 0.0001$, or $c = 0.56207 \pm 0.00005$.

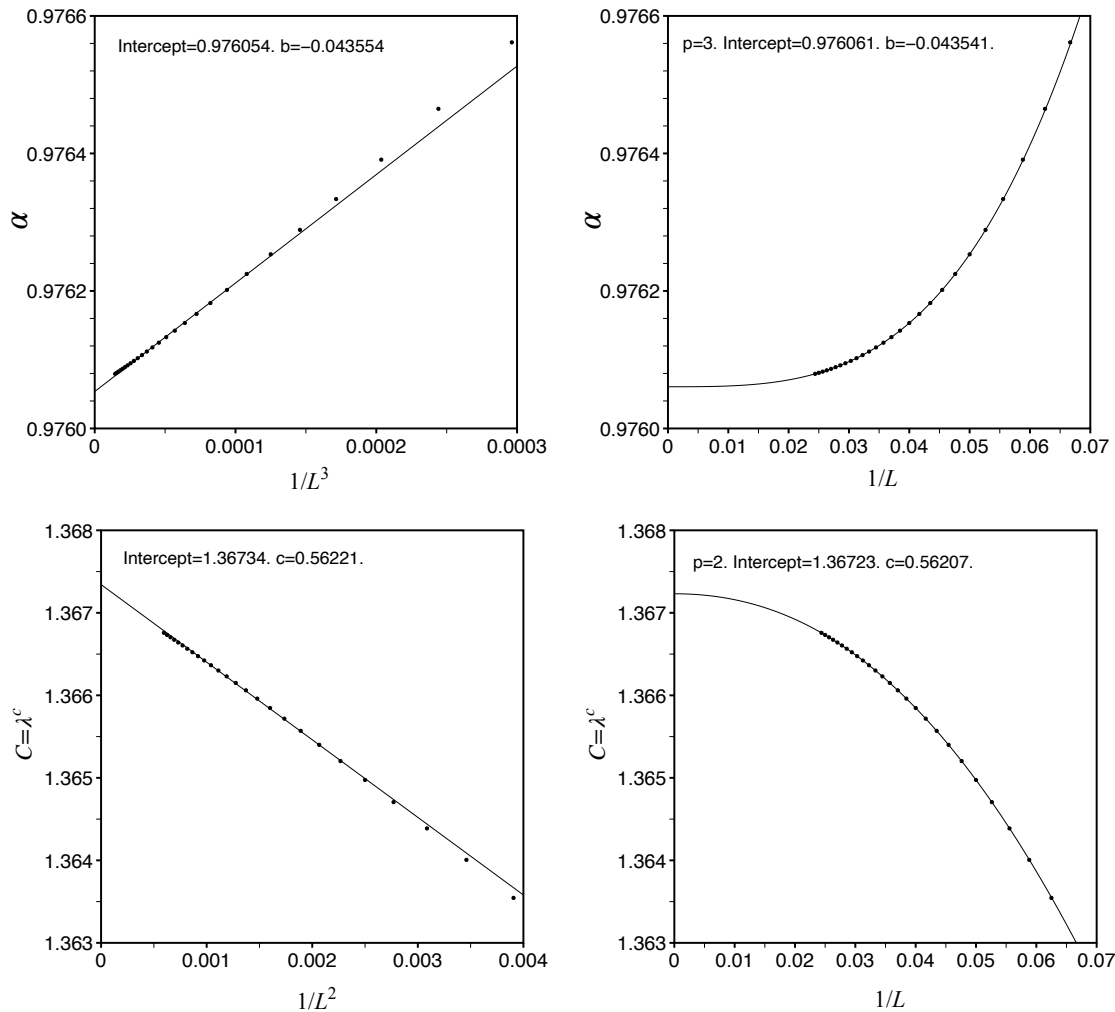


Figure 10: Ratios $d_L/d_{L-1} \sim \alpha$ plotted against $1/L^3$ (top-left) and the amplitude $C = \lambda^c$ plotted against $1/L^2$ (bottom-left). The panels on the right display the same data plotted against $1/L$ with the solid curve being a least-squares fit.

We now turn to the second method P2 to obtain estimates of the parameters $b \log \lambda_S$, $c \log \lambda_S$, and g . As was the case above, these estimators have a lot of curvature when plotted against $1/L$. Hence we plotted against integer powers p of $1/L$ until we found a value for which approximate linearity was achieved and we then performed a least-squares fit to the data to the form $c_0 + c_p/L^p + c_{p+1}/L^{p+1} + c_{p+2}/L^{p+2}$. Plots of these against $1/L$ are shown in the first three panels of Figure 11. From these plots, we estimate

$b \log \lambda_S = -0.02422 \pm 0.00002$, or $b = -0.04353 \pm 0.00002$, $c \log \lambda_S = 0.314 \pm 0.001$, or $c = 0.564 \pm 0.002$, and $g \approx 0$. The agreement between the two methods is excellent and well within quoted confidence limits.

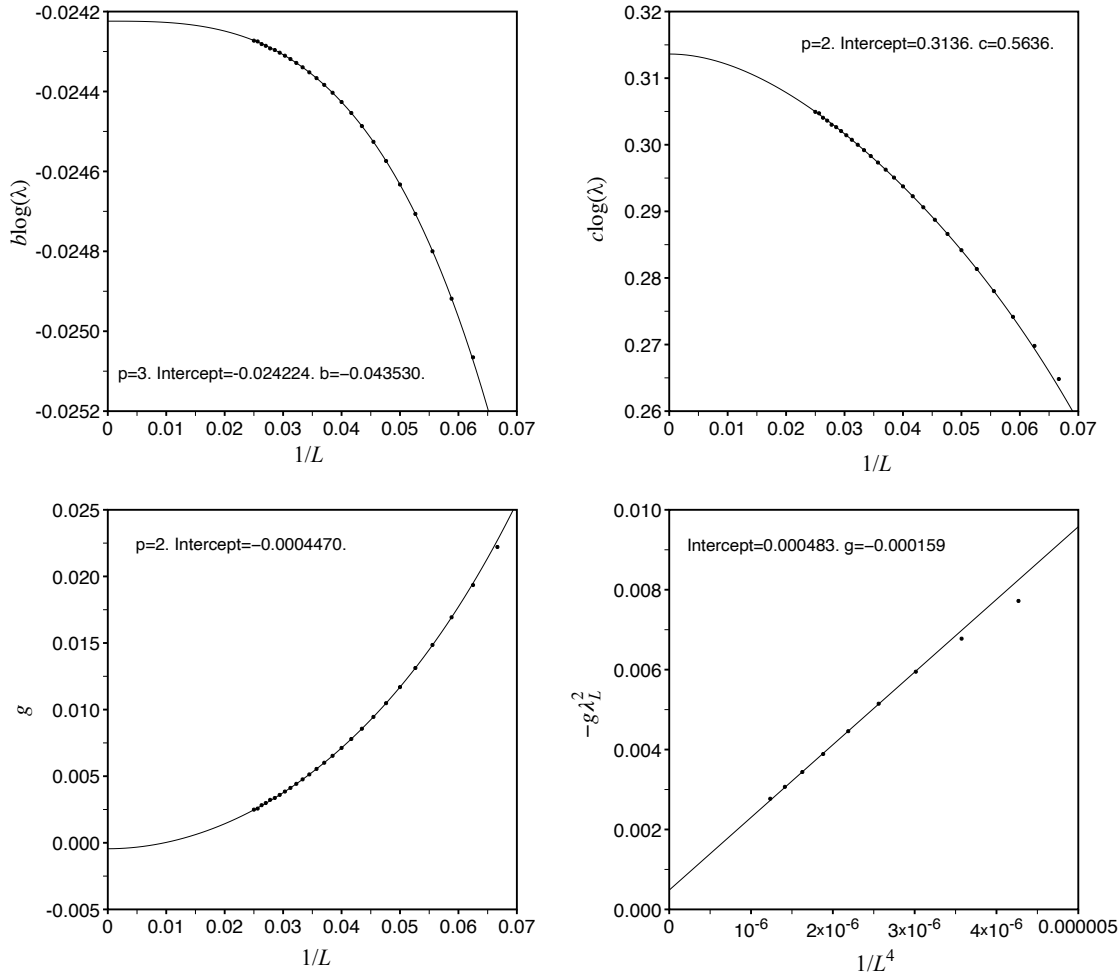


Figure 11: Estimators of $b \log \lambda_S$, $c \log \lambda_S$, and g from method P2 plotted against $1/L$, and the estimator $-g \lambda_L^2$ from method P3 plotted against $1/L^4$.

Accordingly we conclude that our analysis has provided overwhelming numerical evidence that the conjectured asymptotic form

$$C_L(1) \sim \lambda_S^{L^2+bL+c} \cdot L^g,$$

is correct. For SAWs crossing a square we estimate (conservatively) that the parameters take the values $\lambda_S = 1.7445498 \pm 0.0000012$, $b = -0.04354 \pm 0.0001$, $c = 0.5624 \pm 0.001$, and $g = 0.000 \pm 0.005$.

Next we use differential approximants to analyse the series $\mathcal{R}(z) = \sum R_L z^L$. We show the results of the analysis, using 3rd order differential approximants (and of course only the exactly known 27 terms) in Table 2. From this we estimate the radius of convergence as $z_c = 1/\lambda_S^2 = 0.3285735 \pm 0.000001$, which gives $\lambda_S = 1.744551 \pm 0.000003$.

L	Singularity	Exponent
0	0.3285739(14)	-0.99989(27)
1	0.32857478(95)	-1.00010(18)
2	0.32857481(99)	-1.00012(20)
3	0.3285745(10)	-1.00007(21)
4	0.3285746(24)	-1.00004(42)
5	0.3285730(49)	-0.9998(10)
6	0.3285745(18)	-1.00004(38)

Table 2: Estimates of the singularity and exponent of the sequence for the ratios of walks crossing a square series. The estimates are from third order differential approximants with various degrees L of the inhomogeneous polynomial.

(n, m)	Root	(n, m)	Root	(n, m)	Root
(8,8)	1.7445242860	(8,10)	1.7445439450	(8,12)	1.7445454270
(10,8)	1.7445415440	(10,10)	1.7445441380	(10,12)	1.7445488060
(12,10)	1.7445497750	(12,12)	1.7445487670	(12,14)	1.7445489710
(13,11)	1.7445488890	(13,13)	1.7445491150	(14,12)	1.7445491730

Table 3: Estimates of λ_S obtained from Padé approximants.

This is slightly less precise than the ratio methods. The estimates for the critical exponent are clearly supportive of $\mathcal{R}(z)$ having a simple pole adding even more evidence to the validity of the assumed asymptotic form.

We also tried using Padé approximants to estimate λ_S . In Table 3 we list some estimates of λ_S obtained from $P_{m,n}(z)$ Padé approximants to $\mathcal{R}(z)$ by calculating the real roots of the denominator polynomial $Q_n(z)$, finding the smallest positive root to obtain an estimate of λ_S . It is clear that this method works just fine but it is, perhaps not surprisingly, at least an order of magnitude less accurate than differential approximants let alone the ratio methods. Hence we shall not consider this method or differential approximants any further.

Finally, we turn to the analysis of $\mathcal{R}(z)$ using biased differential approximants (see Appendix B.1). We pick a biasing value $\hat{\lambda}_S$ and force the differential approximants to have a singularity of order 1 at $z_c = 1/\hat{\lambda}_S^2$. We calculate many (> 100) 3rd order biased differential approximants with an inhomogeneous polynomial of degree K , such that the number of required terms of the approximants $N \geq 22$. Each approximant in turn provides us with an estimate of the critical exponent γ , which we confidently conjecture has the value -1 . From all of these γ estimates we discard the outlying 10% on either side. The remaining estimates are used to calculate the mean and standard deviation. This procedure is then repeated for different values of $\hat{\lambda}_S$ so as to cover the full range of values within our estimated range $\lambda_S = 1.7445498 \pm 0.0000012$. In Figure 12 we show

a plot of the γ estimates (with error-bars) as a function of $\hat{\lambda}_S$ for the two cases where the degree of the inhomogeneous polynomial is 0 and 4, respectively. We notice that the curve of exponent estimates intersects $\gamma = -1$ over a very narrow range (smaller than the error estimate on λ_S). Obviously it is very tempting to try and use this to provide an even more precise estimate of λ_S . One may say that λ_S could be estimated from the crossing with an error given by the width of the range over which error-bars on the exponent estimates overlap with $\gamma = -1$ (or perhaps a factor of two or three times this range). However, this is a very new method and we are not yet confident that it is a valid method for obtaining more accurate estimates of critical points in cases where the exponent is known exactly. In particular we have no real idea of how to confidently estimate an error-bar. All we are willing to say at the moment is that it appears to be a promising method that warrants further detailed investigation.

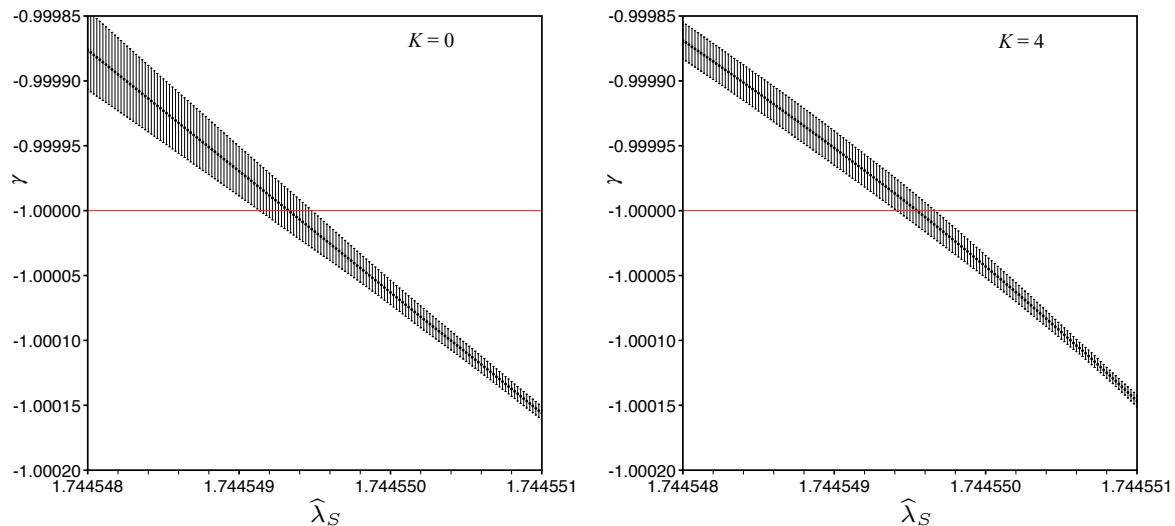


Figure 12: Biased estimators for the critical exponents γ of $\mathcal{R}(z)$ plotted against the biasing value $\hat{\lambda}_S$.

4.2. Polygons crossing a square

Using the algorithm described in Section 2 we calculated $P_L(1)$ to lattice size $L = 26$ and we then used the method of series extension to obtain a further 30 approximate terms.

We first estimated λ_S by method M1, that is extrapolating the sequence $\lambda_L = P_L(1)^{1/L^2}$ against $1/L$. There was some curvature in the plot, so we extrapolated against $c_0 + c_1/L + c_2/L^2 + c_3/L^3$. In this case the estimates appear fairly straight when plotted against $1/L^2$ as shown in the left panel of Figure 13. From this plot we estimate that $\lambda_S = 1.744550 \pm 0.000005$. Next we used method M2, that is we looked at the ratio of ratios. We extrapolated against $c_0 + c_2/L^2 + c_3/L^3$, and plotted this against $1/L^4$ as shown in the right panel of Figure 13. This allowed us to estimate $\lambda_S^2 = 3.043454 \pm 0.000003$, and hence $\lambda_S = 1.7445498 \pm 0.0000008$, in agreement with the previous analysis.

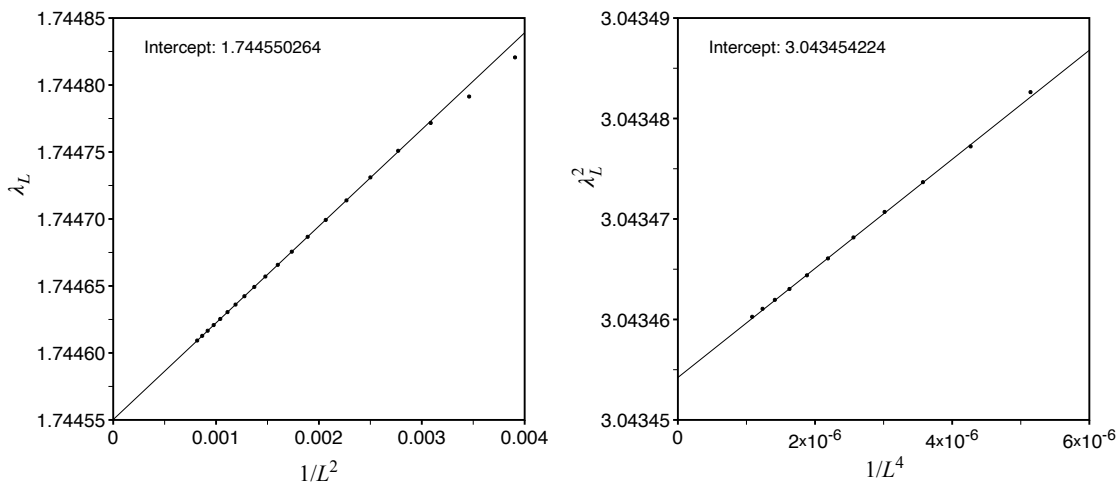


Figure 13: Estimators of λ_S from method M1 plotted against $1/L^2$ and λ_S^2 from method M2 plotted against $1/L^4$.

We estimated the values of the sub-dominant terms by method P2 and we also estimated g by method P3. The various plots are shown in Figure 14. In this way we estimate $b \log \lambda_S \approx -0.02422$, or $b \approx -0.04352$, $c \log \lambda_S \approx -0.6665$ or $c \approx -1.195$, and $g \approx -0.5005$. From the estimate $-g\lambda_S^2 \approx 1.5235$ we get $g \approx -0.5006$. We conjecture with some confidence that $g = -\frac{1}{2}$, exactly. Using our best estimate for λ_S and our conjecture for the exact value of g we then turned to method P1. The plot of the estimator for α is close to linear against $1/L$, but to account for small correction we used a least-squares cubic fit in $1/L$ (solid curve) and found from the intercept that $\alpha = \lambda_S^b \approx 0.9761$ and hence $b \approx -0.04351$. We next make use of the intercept value from the α -plot to estimate c . We look at the quantity $C = \lambda_S^c \sim d_L/(\alpha^L L^g)$, plot it against $1/L$, and use a cubic least-square fit to estimate the intercept $C \approx 0.5130$ and hence $c \approx -1.199$. The parameter estimates from the various method are in good agreement and clearly it seems that b has the same value as for walks crossing a square.

4.3. Walks spanning a square

We calculated $C_L(1)$ to lattice size $L = 26$ and we then used the method of series extension to obtain a further 30 approximate terms. The plots used to estimate the parameters of this model are shown in Appendix E Figure E1. We estimate $\lambda_S \approx 1.74455$ from method M1 using a fourth degree estimator and $\lambda_S^2 \approx 3.043455$ (and hence $\lambda_S \approx 1.744550$) from method M2 fitting to a cubic polynomial. We estimated the values of the sub-dominant terms by method P2, and we also estimated g by method P3. We estimate $b \approx -0.0435$, $c \approx 0.603$, and $g \approx 1.74$. From the estimate $-g\lambda_S^2 \approx -5.33$ we get $g \approx 1.75$. It seems reasonable to conjecture that $g = \frac{7}{4}$, exactly. We finally used this value of g in method P1 and we found $b \approx -0.0435$ and $c \approx 0.4088$. Our estimates for b and g are in agreement and b again has the same value as for walks crossing a square, but there is quite a variation in our estimates of c .

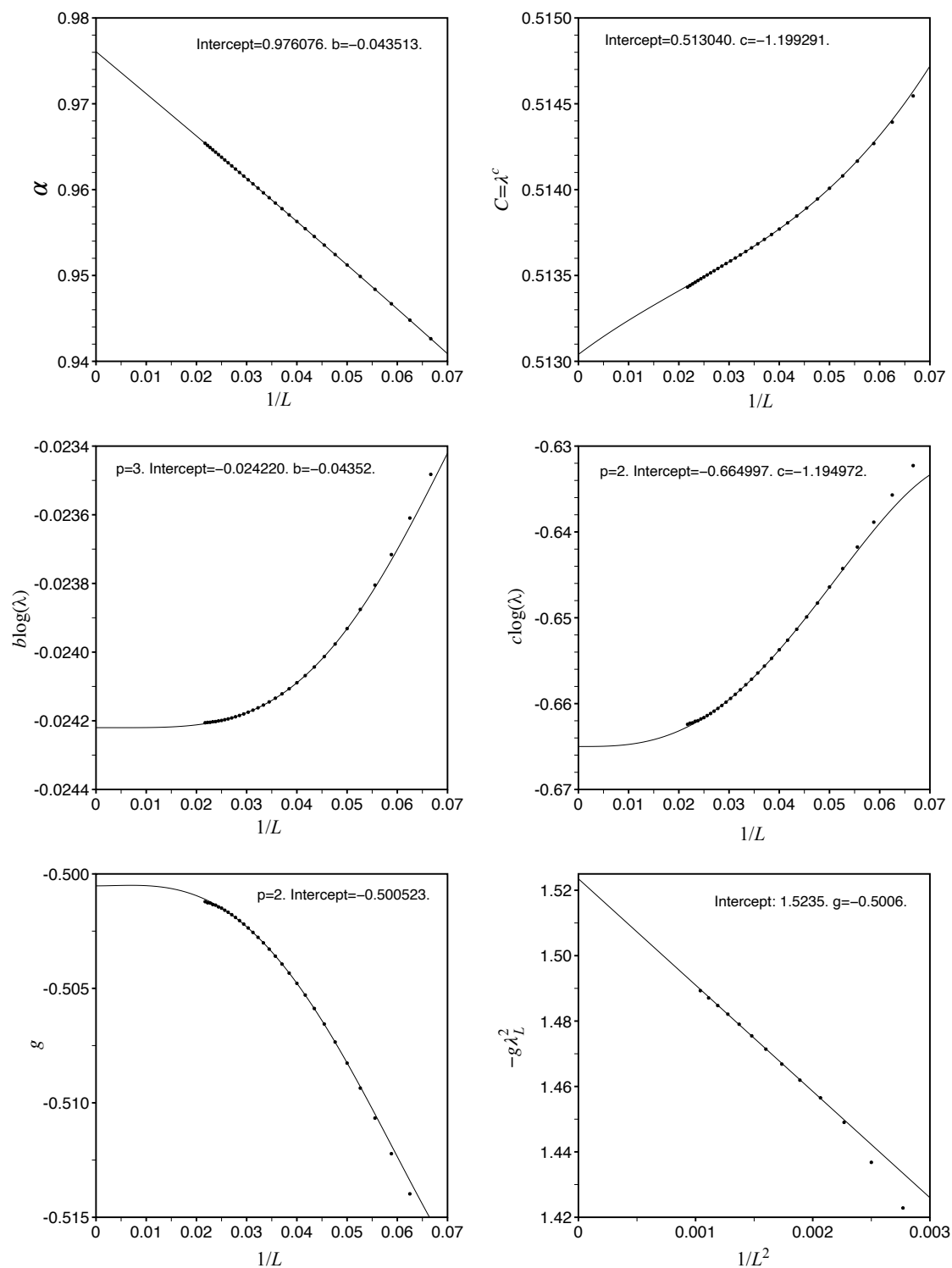


Figure 14: Plots of the estimators for parameters α and $C = \lambda_S^c$ from method P1, $b \log \lambda_S$, $c \log \lambda_S$, and g from method P2 and the estimator $-g \lambda_L^2$ from method P3 for polygons crossing a square.

5. Walks crossing a domain of the hexagonal lattice.

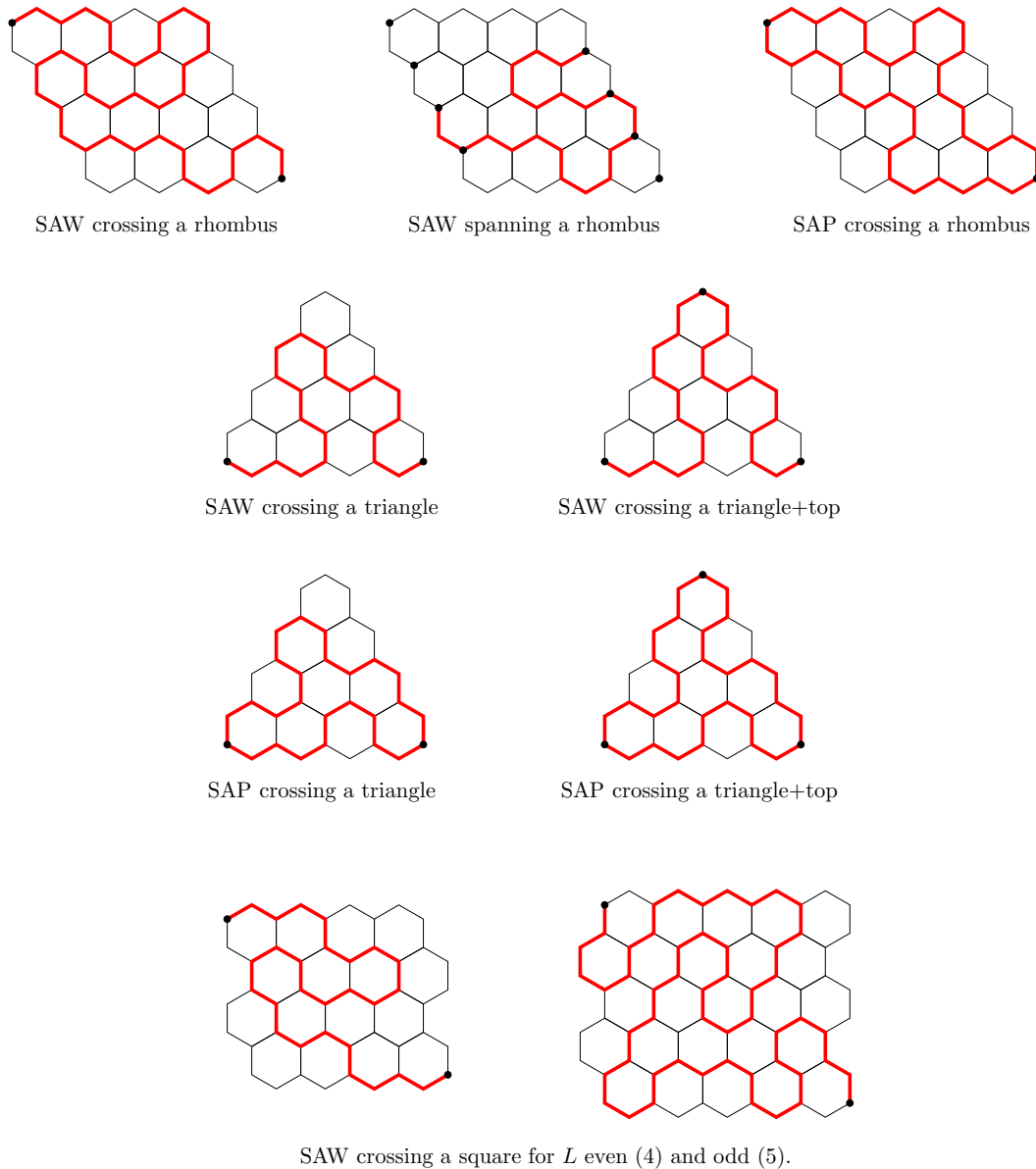


Figure 15: Classes of walk and polygon configurations investigated.

In this section we study walks and polygons crossing a specified domain of the hexagonal lattice. We study several different variants of the problem, including both SAWs and SAPs, on triangular, rhomboidal domains and and SAWs on square domains. These are illustrated in Figure 15. We expect that the number of walks $C_L(1)$ for all these cases will have the asymptotic form (2). More specifically the number of walks should have dominant asymptotic growth determined by

$$C_L(1) \sim \kappa^{\# \text{ vertices in domain}}.$$

The number vertices in a triangular domain of size L is $L^2 + 4L + 1$, while there are $2L^2 + 4L - 1$ vertices in the rhomboidal and square domains. Hence, we expect there to be a common growth constant λ_H such that $\kappa = \lambda_H$ for the triangular domain and $\kappa = \lambda_H^2$ for the rhomboidal and square domains. The other parameters, b , c and g , in the asymptotic form (2) may differ from problem to problem.

In all cases we used the method of series extension to obtain further *approximate* terms from the known exact terms by using differential approximants to predict further coefficients, as described in Appendix C. How many further terms can be obtained varies from problem to problem and in each case we take all predicted coefficients whose spread among estimates (as measured by 1 standard deviation) is less than 1 part in 10^5 . In this way we expect the least accurate coefficients to be accurate to around 1 part in 10^5 . As a consequence, we expect that simple ratio plots will be smooth and indistinguishable from those obtained by the exact coefficients. However when we use more elaborate calculations, such as extrapolating against a polynomial in $1/L$, that operation magnifies the errors. This is made manifest by smooth plots starting to display irregularities. Accordingly, we cut off such values, and don't use these less accurate coefficients in those plots. To be more specific, if we extend a series by, say, 60 terms, we will use them all in a ratio plot, but when fitting to say, $c_0 + c_1/L + c_2/L^2 + c_3/L^3$, we may only use the first 30 extra coefficients. Method M2 is particularly sensitive and we could often only make use of as few as 4 of the approximate terms.

5.1. Self-avoiding walks crossing a triangle.

The paths we are counting are shown in Figure 15. Using the algorithm described in Section 2 we calculated $C_L(1)$ to lattice size $L = 27$ and we then used the method of series extension to obtain a further 60 terms. We first estimated λ_H by method M1, that is extrapolating the sequence $\lambda_L = C_L(1)^{1/L^2}$ against $1/L$. There was some curvature in the plot, so we extrapolated against $c_0 + c_1/L + \dots + c_m/L^m$, which allowed us to make a rather precise estimate, $\lambda_H = 1.3872495 \pm 0.0000005$. We show, in Figure 16, just how well-converged this data is. We next considered the sequence $\{C_L\}$ which plotted against $1/L^2$ is an almost straight line. We then fitted the sequence to $c_0 + c_2/L^2 + c_3/L^3$. This gave exceptionally good apparent precision, allowing for a very precise estimate. We estimate $\lambda_H^2 = 1.9244612 \pm 0.0000002$, or $\lambda_H = 1.38724951 \pm 0.00000001$. The plots are shown in Figure 17.

We estimated the values of the sub-dominant terms by method P2, fitting successive coefficients to

$$\log d_L \sim b \log(\lambda_H)L + c \log(\lambda_H) + g \log L,$$

and we estimated $-g\lambda_H^2$ from the cubic fit to the sequence $\{C_L\}$. The relevant plots are shown in Figure 18. In this way we estimate $b \approx 0.4443$, $c \approx 0.924$, $g \approx 0.0834$, and $-g\lambda_H^2 \approx -0.1602$, so $g \approx 0.0832$, which is suggestive of the exact fraction $1/12$. This exponent value was then used in method P1 from which we estimate $b \approx 0.4442$ and $c \approx 0.9214$ in good agreement with the results of method P2.

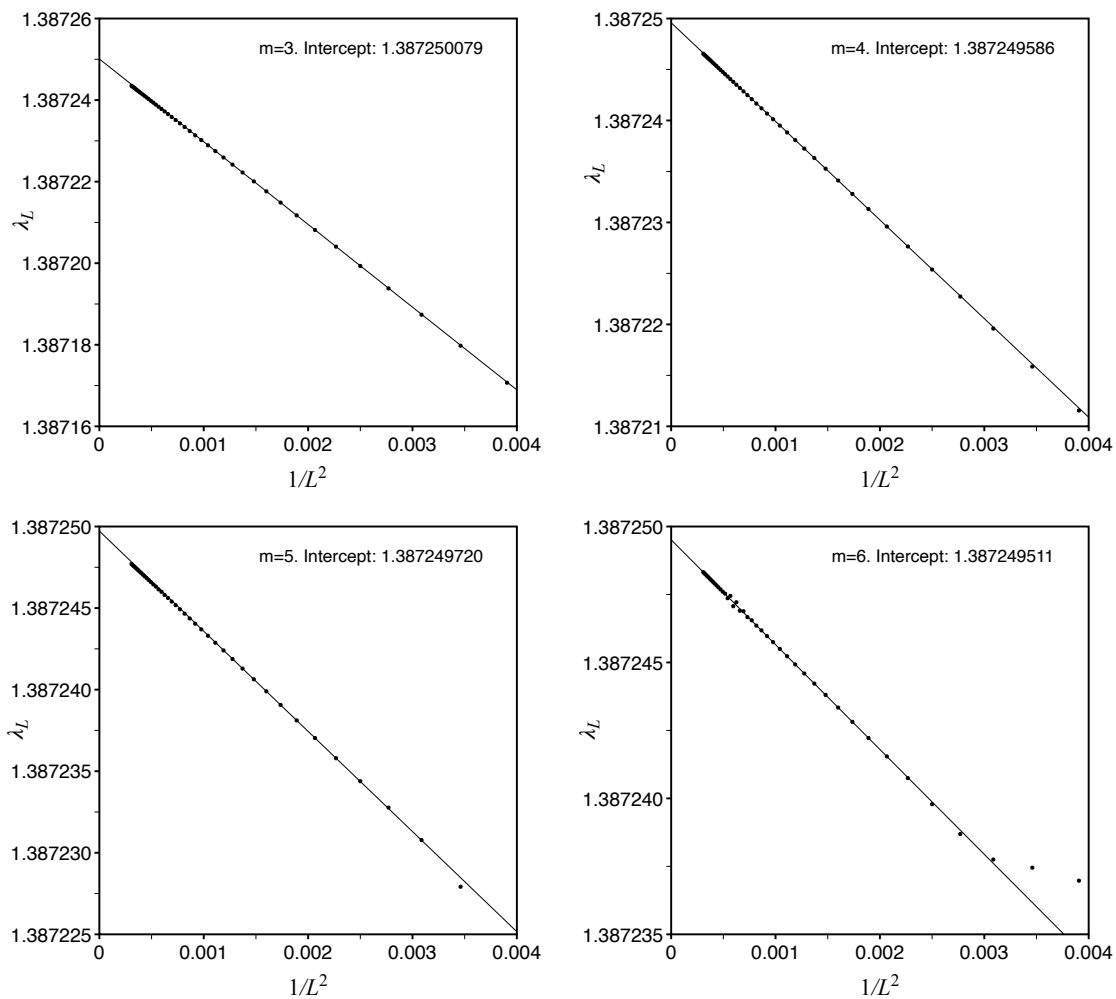


Figure 16: Estimators of λ_H from method M1 when fitting against polynomials in $1/L$ of degree $m = 3$ to 6 for SAWs crossing a triangle.

Finally we display in Figure 19 the results from a biased differential approximant analysis of $\mathcal{R}(z)$. The biased estimates of γ cross the value -1 in a very narrow range very close to our estimate $\lambda_H \approx 1.38724951$ from the previous analysis.

We therefore conclude that for SAWs crossing a triangular domain of the hexagonal lattice we have found very firm numerical evidence that the conjectured asymptotic form (2) is correct and we estimate that the parameters have the values $\lambda_H = 1.38724951 \pm 0.00000005$, $b = 0.4443 \pm 0.001$, $c = 0.923 \pm 0.005$, and $g = 0.0833 \pm 0.0005$, where possibly $g = 1/12$ exactly.

5.2. Self-avoiding walks crossing a rhombus.

The paths we are counting are shown in Figure 15. We calculated $C_L(1)$ to lattice size $L = 26$ and then extended this sequence by a further 50 terms. We first estimated λ_H^2 using method M1 by extrapolating against $c_0 + c_1/L + \dots + c_m/L^m$, as shown in Figure 20 for $m = 3$ to 6. From this we estimate that $\lambda_H^2 = 1.924461 \pm 0.000002$, or

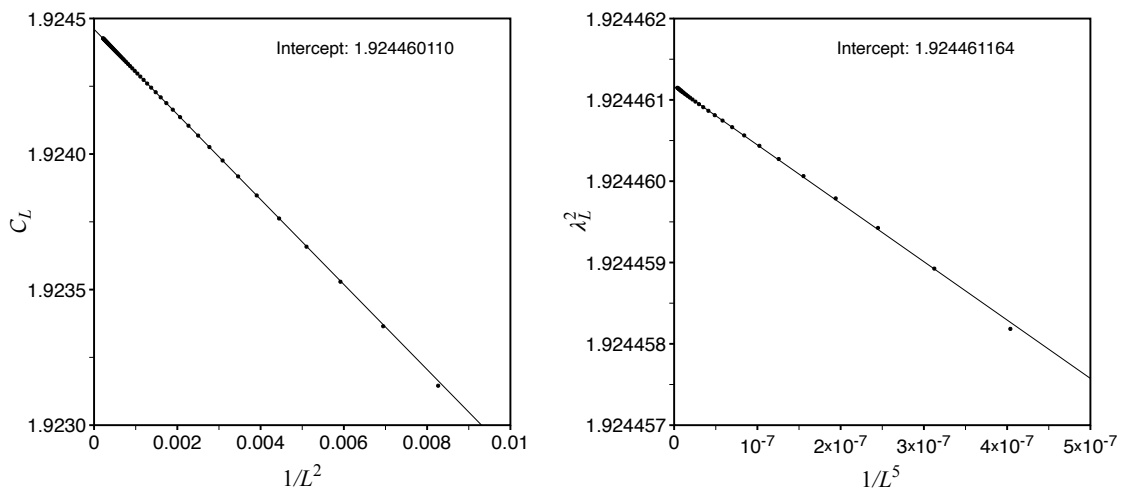


Figure 17: C_L plotted against $1/L^2$ and the estimator λ_L^2 from method M2 with a cubic fit plotted against $1/L^5$ for SAWs crossing a triangle.

$\lambda_H = 1.3872494 \pm 0.000008$. Next we used method M2 to obtain an estimate for λ_H^4 . In Figure 21 we show a plot of C_L plotted against $1/L^2$ and the estimates obtained by fitting the sequence $\{C_L\}$ to $c_0 + c_2/L^2 + c_3/L^3$. We estimate $\lambda_H^4 = 3.7035506 \pm 0.0000006$, or $\lambda_H = 1.3872498 \pm 0.00000006$. These estimates for λ_H are consistent with the estimate obtained above for the triangular domain.

We estimated the values of the sub-dominant terms by method P2, fitting successive coefficients to

$$\log d_L \sim 2b \log(\lambda_H)L + 2c \log(\lambda_H) + g \log L,$$

and we estimated $-g\lambda^2$ from the cubic fit to the sequence $\{C_L\}$. The relevant plots are shown in Figure 22. We estimate $b \approx -0.3705$, $c \approx 0.6258$, $g \approx 0.167$, and $-g\lambda_H^2 \approx -0.615$, so $g \approx 0.166$, which is suggestive of the exact fraction $1/6$. From method P1 we then obtained the estimates $b \approx -0.3707$ and $c \approx 0.6266$.

Finally we display in Figure 23 the results from a biased differential approximant analysis of $\mathcal{R}(z)$. Once again we see that the biased estimates of γ cross the value -1 in a narrow range contained within our best estimate $\lambda_H \approx 1.38724951 \pm 0.00000005$.

Hence, SAWs crossing a rhomboidal domain of the hexagonal lattice follows the conjectured asymptotic form (2) with growth constant λ_H^2 and sub-dominant parameters $b = -0.3706 \pm 0.0005$, $c = 0.6262 \pm 0.001$, and $g = 0.167 \pm 0.002$, where possibly $g = 1/6$.

5.3. SAWs spanning a rhombus

We have series to lattice size $L = 26$ and we managed to obtain a further 37 approximate terms. Method M1 with a degree six polynomial extrapolation allowed us to make the estimate $\lambda_H^2 = 1.92446 \pm 0.00003$, or $\lambda_H = 1.38725 \pm 0.00001$. From method M2 and P3 with a cubic fit we estimate $\lambda_H^4 = 3.703551 \pm 0.000005$, or $\lambda_H = 1.3872495 \pm 0.0000005$, and $-g\lambda_H^4 \approx -6.18$, so $g \approx 1.67$. From method P2 we estimate $b \approx -0.3705$, $c \approx 1.44$,

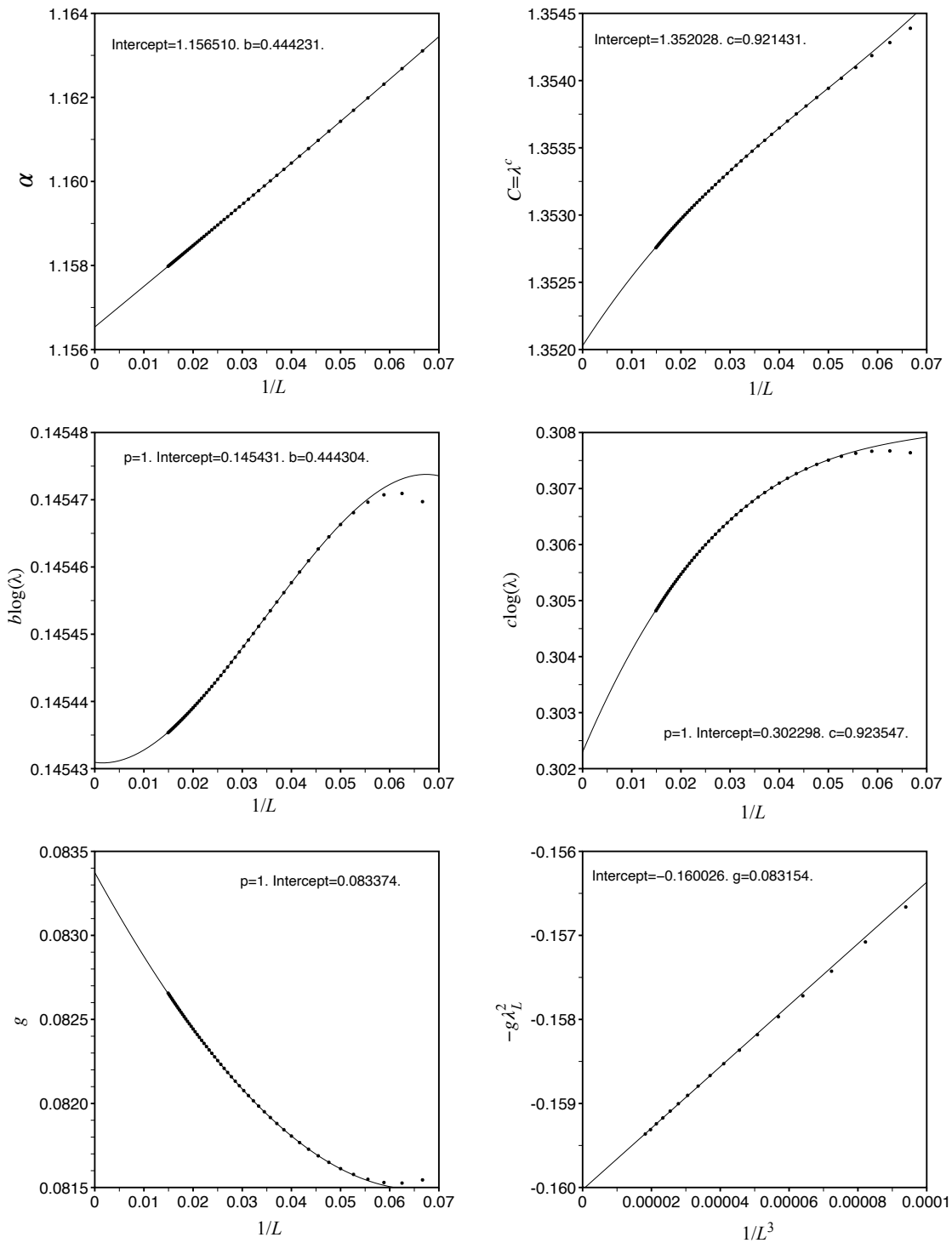


Figure 18: Estimators of α and $C = \lambda^c$ from method P1, $b \log \lambda_S$, $c \log \lambda_S$, and g from method P2, and the estimator $-g\lambda_L^2$ from method P3 for SAWs crossing a triangle.

and $g \approx 1.675$, in precise agreement with the estimate from method P3. We suggest that perhaps $g = \frac{5}{3}$. Method P1 then yielded the estimates $b \approx -0.3706$ in agreement with the previous estimate and $c \approx 1.56$ somewhat large but still consistent with the estimate

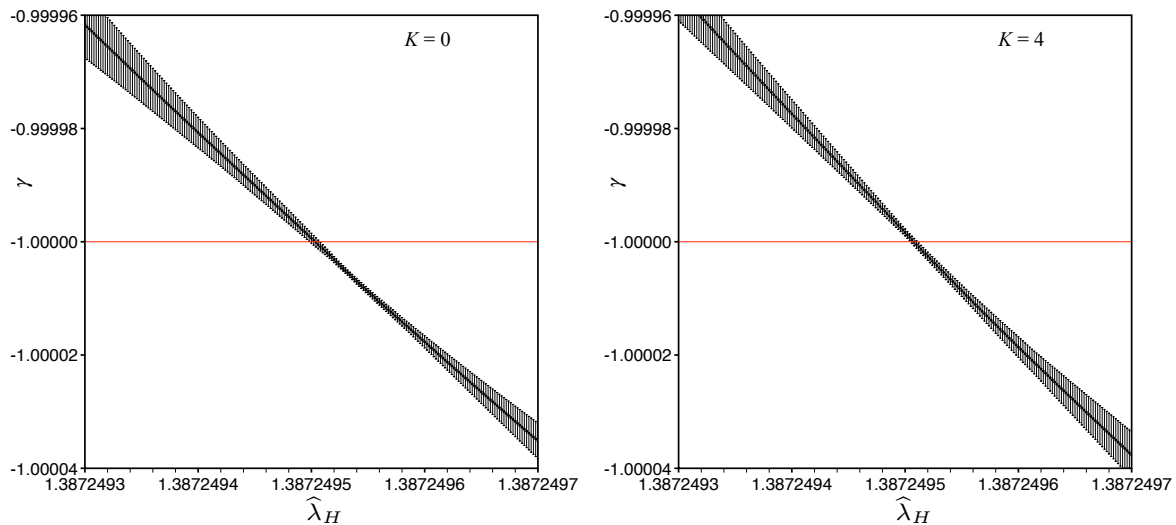


Figure 19: Biased estimates for the critical exponent γ of $\mathcal{R}(z)$ plotted against the biasing value $\hat{\lambda}_H$ for SAWs crossing a triangle.

from method P2. The plots can be seen in Figure E2.

5.4. Polygons crossing a rhombus

We calculated series to lattice size $L = 26$ and extended by 60 approximate terms. Method M1 yielded the estimate $\lambda_H^2 = 1.92446 \pm 0.00001$ ($\lambda_H = 1.387249 \pm 0.000005$) and method M2 and P3 $\lambda_H^4 = 3.7035515 \pm 0.0000015$ ($\lambda_H = 1.38724956 \pm 0.00000015$) and $-g\lambda_H^2 \approx 2.157$, so $g \approx -0.583$, where in each method we used a cubic extrapolation of the sequence. This is clear evidence that the growth parameter λ_H for polygons is the same as for SAWs, which is to be expected. Method P2 was again used to estimate the values of the sub-dominant terms and we estimate $b \approx -0.3705$, $c \approx -1.0543$, and $g \approx -0.583$, in agreement with the estimate from method P3. We hazard the guess that $g = -7/12$, exactly. From method P1 we then estimated $b \approx -0.3705$ and $c \approx -1.0529$. The plots can be seen in Figure E3.

5.5. Self-avoiding walks crossing a triangle and passing through the top vertex.

We calculated $C_L(1)$ to lattice size $L = 26$ and extended the series by a further 60 approximate terms. We estimated λ_H , by method M1 where an extrapolation of degree six allowed us to estimate $\lambda_H = 1.3872495 \pm 0.0000005$. Using method M2 we estimated $\lambda_H^2 = 1.9244611 \pm 0.0000001$ ($\lambda_H = 1.38724947 \pm 0.00000005$) and $-g\lambda_H^2 \approx -0.160$, so $g \approx 0.0831$, in agreement with the value found for SAWs crossing a triangle. We estimated the values of the sub-dominant parameters by method P2 and we found $b \approx 0.4443$, $c \approx -1.7861$, and $g \approx 0.0833$, in good agreement with the estimate given immediately above, and suggestive of an exact fraction $1/12$. Method P1 yielded the estimates $b \approx 0.4442$ and $c \approx -1.7891$ in agreement with the previous estimates. The

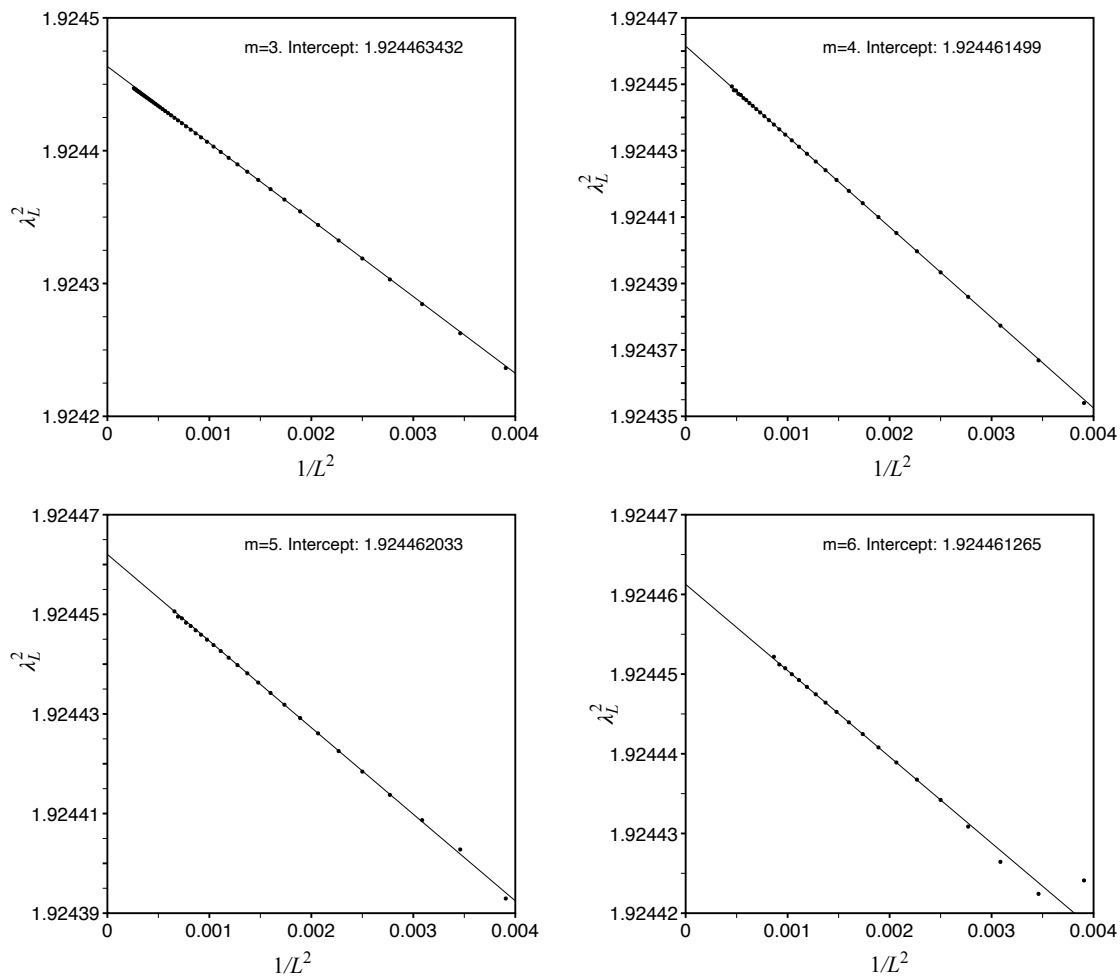


Figure 20: Estimators of λ_H from method M1 when fitting against polynomials in $1/L$ of degree $m = 3$ to 6 for SAWs crossing a rhombus.

plots can be seen in Figure E4.

5.6. Polygons in a triangle.

We define $P_L(1)$ as the number of polygons in a triangular domain passing through two of the three corner vertices as shown in Figure 15. We calculated series to lattice size $L = 26$ and obtained a further 50 approximate terms. We first estimated λ_H , by method M1 and found $\lambda_H = 1.387245 \pm 0.000002$. Method M2 gave good apparent precision, giving us the precise estimate $\lambda_H^2 = 1.924461 \pm 0.000001$ ($\lambda_H = 1.3872494 \pm 0.0000004$) and from method P3 we found $-g\lambda_H^2 \approx 1.282$, so $g \approx -0.666$, which is very suggestive of the exact fraction $-2/3$. We estimated the values of the sub-dominant terms from method P2 and found $b \approx 0.4443$, $c \approx -1.394$, and $g \approx -0.666$, in total agreement with the estimate of g given immediately above. Method P1 gave $b \approx 0.4443$ and $c \approx -1.380$ in good agreement with the previous analysis. The plots can be seen in Figure E5.

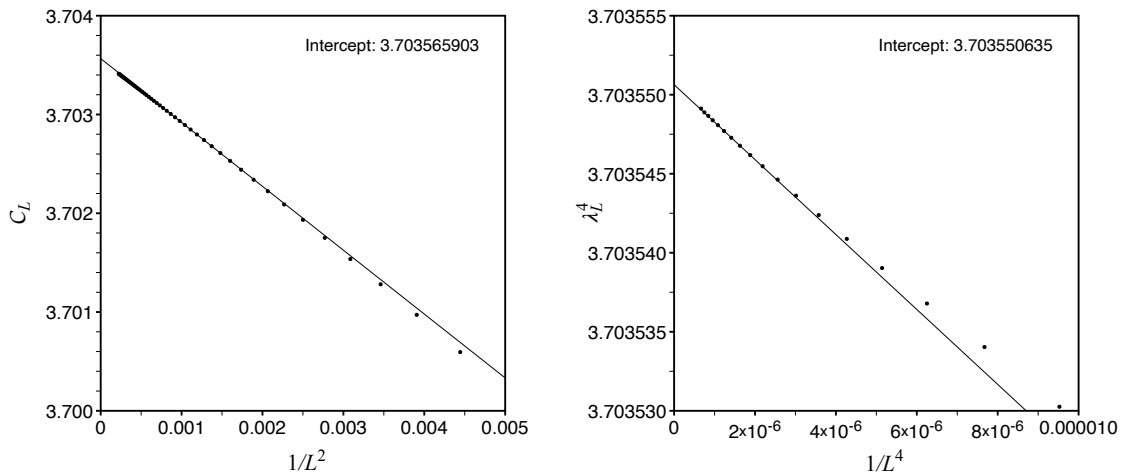


Figure 21: C_L plotted against $1/L^2$ and the estimator λ_L^4 from method M2 with a cubic fit plotted against $1/L^4$ for SAWs crossing a rhombus.

5.7. Polygons in a triangle passing through the top vertex.

We define $P_L(1)$ as the number of polygons in a triangular domain passing through all three corner vertices of the domain as illustrated in Figure 15. The series was calculated to lattice size $L = 26$ and extended by 40 further approximate terms. Method M1 yielded the estimate $\lambda_H = 1.38725 \pm 0.00001$ and method M2 gave $\lambda_H^2 = 1.924461 \pm 0.000002$ ($\lambda_H = 1.38725 \pm 0.00001$) while method P3 gave $-g\lambda_H \approx 1.284$, so $g \approx -0.667$. Method P2 resulted in the estimates $b \approx 0.4443$, $c \approx -4.106$, and $g \approx -0.667$. We conjecture $g = -2/3$ exactly. Method P1 resulted in the estimates $b \approx 0.4443$ and $c \approx -4.091$ in agreement with the previous results. The plots can be seen in Figure E6.

5.8. SAWs crossing a square

The paths we are counting are shown in Figure 15. We calculated series to lattice size $L = 24$ and we extended the series by a further 25 approximate terms. A consequence of the lattice geometry is that different paths had to be counted according as the lattice size L was odd or even, as shown in Figure 15. This induced a period-2 oscillation in the ratios and other parameters. To accommodate this we redefined the ratios as the square-root of the ratio of alternate terms. That is to say, the ratio $r_L = \sqrt{C_L(1)/C_{L-2}(1)}$. Similarly, when attempting to extrapolate the sequence $\lambda_L = C_L(1)^{1/L^2}$ against a polynomial in $1/L$ we used tuples of alternate terms, rather than successive terms. Even after this adjustment the estimates of λ_L showed some parity effects. Hence we decided to look at the average of consecutive terms, that is, $(\lambda_L + \lambda_{L-1})/2$. Similar changes were made for all the other parameter estimators. The resulting plots are shown in Figure E7

This allowed us to make the precise estimate $\lambda_H^2 = 1.924461 \pm 0.000005$ ($\lambda_H = 1.387249 \pm 0.000003$) from a cubic fit to the sequence $\{C_L(1)^{1/L^2}\}$. When we fitted the sequence $\{C_L\}$ to $c_0 + c_2/L^2 + c_3/L^3$, strong period-2 oscillations required a redefinition,

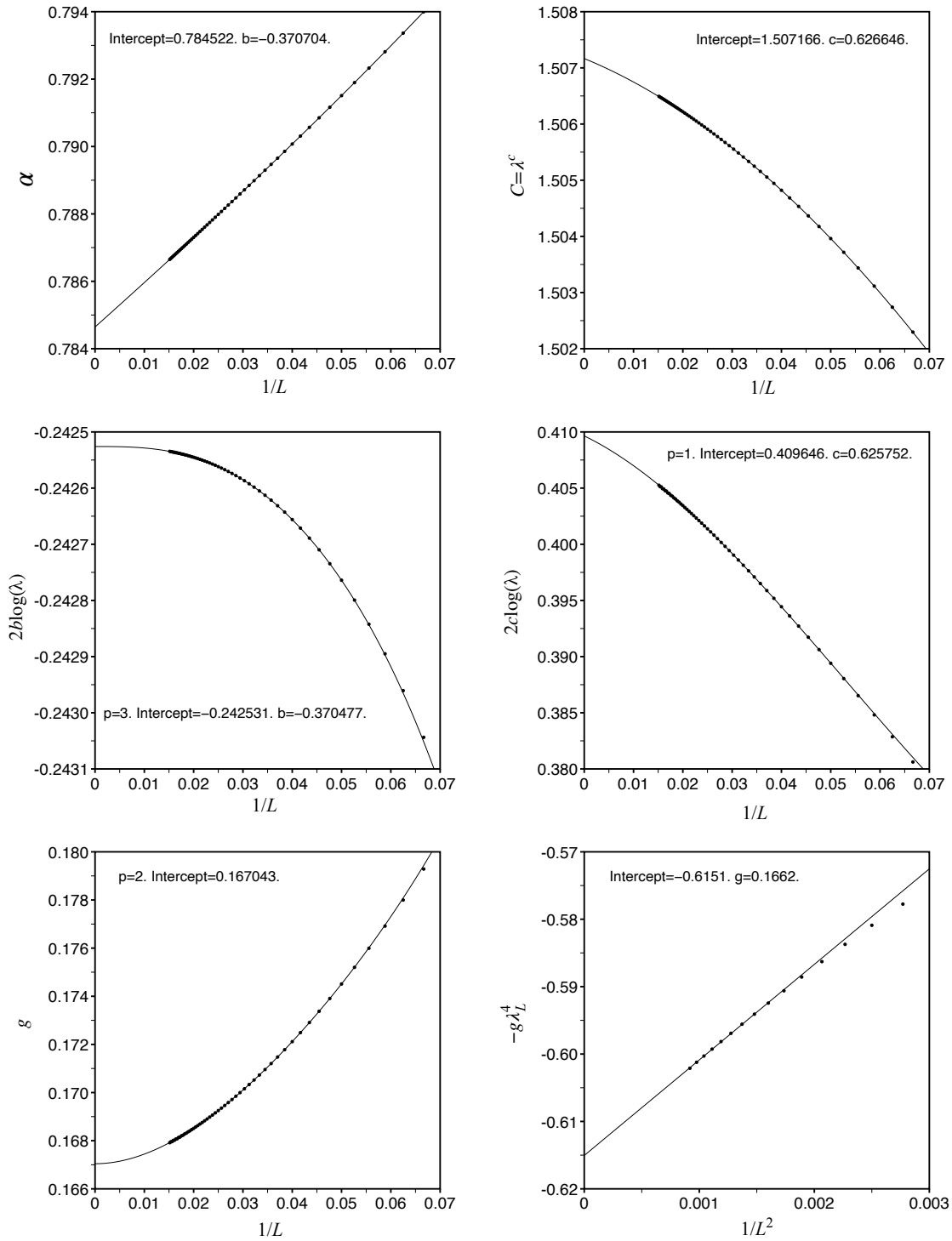


Figure 22: Estimators of α and $C = \lambda^c$ from method P1, $b \log \lambda_S$, $c \log \lambda_S$, and g from method P2, and the estimator $-g\lambda_L^2$ from method P3 for SAWs crossing a rhombus.

so we defined

$$C_L^* := \left(\frac{C_{L-2}(1) \cdot C_{L+2}(1)}{C_L(1)^2} \right)^{1/4}.$$

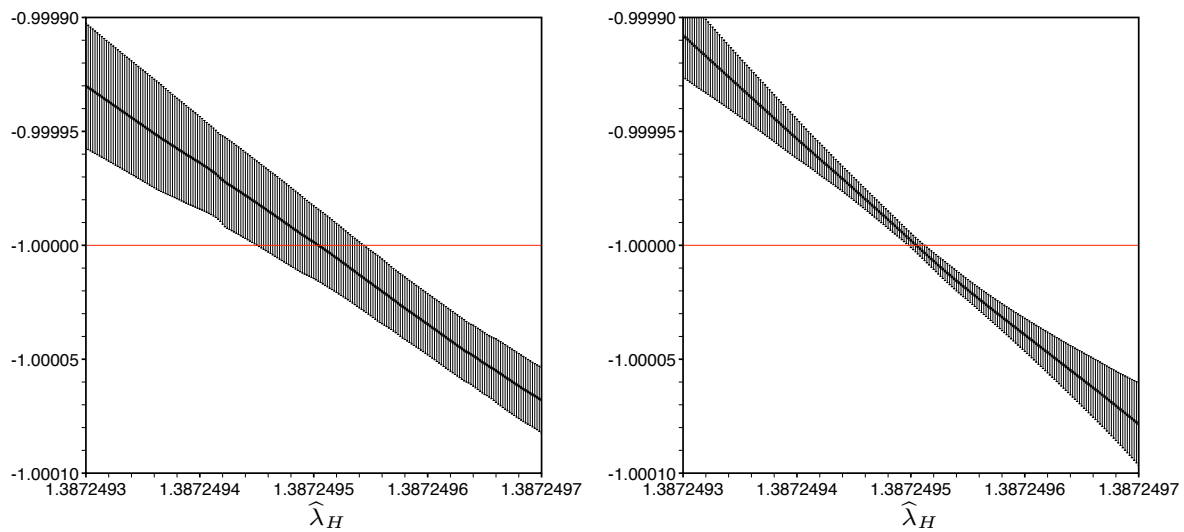


Figure 23: Biased estimates for the critical exponent γ of $\mathcal{R}(z)$ plotted against the biasing value $\hat{\lambda}_H$ for SAWs crossing a rhombus.

As was the case for WCAS this redefined sequence of ratios showed linearity when plotted against $1/L^4$ hence suggesting that $g = 0$ in this case as well. We therefore extrapolated the new sequence against $c_0 + c_4/L^4$, and from a plot against $1/L^7$ we made the estimate $\lambda_H^4 = 3.7035505 \pm 0.0000015$, or $\lambda_H = 1.3872495 \pm 0.0000002$.

We also estimated the values of the sub-dominant terms by method P2 appropriately altered to deal with parity effects. In that way we estimated $b \approx -0.3765$, $c \approx 0.736$, and $g \approx 0.003$, in agreement with $g = 0$. Finally, we used also method P3 to estimate g . Here we fitted the sequence $\{\mathcal{C}_L^*\}$ to $c_0 + c_2/L^2 + c_4/L^4$, so that c_2 becomes an estimator for $-g\lambda_H^4$ and from the plot we estimate that $-g\lambda_H^4 \approx -0.00240$ which again is consistent with the conjecture that $g = 0$ exactly.

6. Conclusion

For SAWs crossing a square on the square lattice, we conjecture that

$$C_L(1) \sim \lambda_S^{L^2 + bL + c} \cdot L^g,$$

where $\lambda_S = 1.7445498 \pm 0.0000012$, $b = -0.04354 \pm 0.0001$, $c = 0.5624 \pm 0.0005$, and $g = 0.000 \pm 0.005$.

For SAWs crossing a closed, connected, convex region on the hexagonal lattice we similarly conjecture $C_L(1) \sim \lambda_H^{L^2}$, where our best estimate of $\lambda_H = 1.38724951 \pm 0.00000005$. For a number of combinatorial problems associated with SAWs on the hexagonal lattice, the growth constant is either known or conjectured. We have not been able to even guess a potential algebraic expression for λ_H that is remotely plausible.

We show in Table 4 our estimates of the parameters b , c , and g for the various geometries and path types we have studied, as well as the conjectured exact values of

Table 4: Estimates of the parameters b , c , and g when fitting to the assumed asymptotic form $C_L(1) \sim \lambda_S^{L^2+bL+c} \cdot L^g$, for the square lattice, $C_L(1) \sim \lambda_H^{2(L^2+bL+c)} \cdot L^g$, for the hexagonal lattice on non-triangular domains, and $C_L(1) \sim \lambda_H^{L^2+bL+c} \cdot L^g$, on triangular domains.

Geometry and lattice	b	c	g and conjecture	
Square lattice				
SAWs crossing a square	-0.04354	0.5624	0	0
SAWs spanning a square	-0.04354	0.5	1.75	7/4
SAPs crossing a square	-0.04354	-1.197	-0.5000	-1/2
Hexagonal lattice				
SAWs crossing a rhombus	-0.3706	0.626	0.167	1/6
SAWs spanning a rhombus	-0.3704	1.78	1.667	5/3
SAPS crossing a rhombus	-0.3705	-1.052	-0.583	-7/12
SAWs crossing a triangle	0.4443	0.923	0.0833	1/12
SAWs crossing a triangle + top vertex	0.4443	-1.787	0.0833	1/12
SAPs crossing a triangle	0.4444	-1.387	-0.666	-2/3
SAPs crossing a triangle + top vertex	0.4443	-4.10	-0.667	-2/3
SAWs crossing a square	-0.3765	0.736	0.003	0

the exponent g . For the hexagonal lattice, it is seen that the parameter b takes one of two values. The value $b \approx -0.3705$ is associated with the rhomboidal geometry, while the value $b \approx 0.4444$ is associated with the triangular geometry. All the exponents g appear to be multiples of $1/12$.

7. Resources

The enumeration data and extended series for all problems studied in this paper, some Maple worksheets used for the asymptotic analysis and some of the source code used to calculate the exact coefficients can be found at our GitHub repository [https://github.com/IwanJensen/Self-avoiding-walks-and-polygons/tree/WCAS\(H\)](https://github.com/IwanJensen/Self-avoiding-walks-and-polygons/tree/WCAS(H)).

Acknowledgements

We would to thank Nathan Clisby for many conversations about the implementation of the perfect hashing algorithm which greatly assisted our efforts and for several helpful suggestions about problems worth studying and for a careful reading of an early version of the manuscript. AJG wishes to thank the ARC Centre of Excellence for Mathematical and Statistical Frontiers (ACEMS) for support.

References

- [1] Guttmann A J and Whittington S G 1990 Self-avoiding walks which cross a square *J. Phys. A: Math. Gen.* **23** 5601–5609.
- [2] Bousquet-Mélou M, Guttmann A J and Jensen I 2005 Self-avoiding walks crossing a square *J. Phys. A: Math. Gen.* **38** 9159–9181.
- [3] Iwashita H, Kawahara J and Minato S 2012 ZDD-based computation of the number of paths in a graph TCS Technical Report TCS-TR-A-12-60 Hokkaido University.
- [4] Iwashita H, Nakazawa Y, Kawahara J, Uno T and Minato S 2013 Efficient computation of the number of paths in a grid graph with minimal perfect hash functions TCS Technical Report TCS-TR-A-13-64 Hokkaido University.
- [5] OEIS Foundation Inc. (2014), The On-Line Encyclopaedia of Integer Sequences, <http://oeis.org>
- [6] Duminil-Copin H and Smirnov S 2012 The connective constant of the honeycomb lattice equals $\sqrt{2 + \sqrt{2}}$ *Ann. Math.* **175** 1653–1665.
- [7] Jacobsen J L, Scullard C R and Guttmann A J 2016 On the growth constant for square-lattice self-avoiding walks *J. Phys. A: Math. Theor.* **49** 494004, (18pp).
- [8] Madras N 1995 Critical behaviour of self-avoiding walks that cross a square *J. Phys. A: Math. Gen.* **28** 1535–1547.
- [9] Abbott H L and Hanson D 1978 A lattice path problem *Ars Combinatoria* **6** 163–178.
- [10] Enting I G 1980 Generating functions for enumerating self-avoiding rings on the square lattice *J. Phys. A: Math. Gen.* **13** 3713–3722.
- [11] Conway A R, Enting I G and Guttmann A J 1993 Algebraic techniques for enumerating self-avoiding walks on the square lattice *J. Phys. A: Math. Theor.* **26** 1519–1534.
- [12] Jensen I 2006 Honeycomb lattice polygons and walks as a test of series analysis techniques *J. Phys.: Conf. Ser.* **42** 163–172.
- [13] Enting I G and Jensen I 2009 Exact Enumerations in *Polygons, Polyominoes and Polycubes* (ed. A J Guttmann) (Heidelberg: Springer) vol. 775 of *Lecture Notes in Physics* chap. 7 143–179.
- [14] Jensen I 2003 A parallel algorithm for the enumeration of self-avoiding polygons on the square lattice *J. Phys. A: Math. Gen.* **36** 5731–5745.
- [15] Nienhuis B 1982 Exact critical point and critical exponents of $O(n)$ models in two dimensions *Phys. Rev. Lett.* **49** 1062–1065.
- [16] Guttmann A J 2016 Series extension: predicting approximate series coefficients from a finite number of exact coefficients *J. Phys. A: Math. Theor.* **49** 415002, (27pp).
- [17] Atapour M and Madras N 2014 Large deviations and ratio limit theorems for pattern-avoiding permutations *Prob. and Comp.* **23** 161–200.
- [18] Guttmann A J 1989 Asymptotic analysis of power-series expansions in *Phase Transitions and Critical Phenomena* (eds. C Domb and J L Lebowitz) (New York: Academic) vol. 13 1–234.
- [19] Forsyth A R 1902 *Part III. Ordinary linear equations* vol. IV of *Theory of differential equations*. (Cambridge: Cambridge University Press).
- [20] Ince E L 1927 *Ordinary differential equations* (London: Longmans, Green and Co. Ltd.)
- [21] Guttmann A J and Jensen I 2009 Series Analysis in *Polygons, Polyominoes and Polycubes* (ed. A J Guttmann) (Heidelberg: Springer) vol. 775 of *Lecture Notes in Physics* chap. 8 181–202.
- [22] Guttmann A J 2015 Analysis of series expansions for non-algebraic singularities *J. Phys. A: Math. Theor.* **48** 045209, (33pp).
- [23] Jensen I 2016 Square lattice self-avoiding walks and biased differential approximants *J. Phys. A: Math. Theor.* **49** 424003 (13pp).

Appendix A. Ratio Method

The ratio method was perhaps the earliest systematic method of series analysis employed, and is still the most useful method when only a small number of terms are known. Given a series $\sum c_n z^n$, which behaves as in eqn. (7), it is assumed that $\lim_{n \rightarrow \infty} c_n/c_{n-1}$ exists and is equal to the growth constant. For some combinatorial sequences such as classical pattern-avoiding permutations of length up to 5, this has been proved by Atapour and Madras [17].

From eqn. (8), it follows that the *ratio* of successive terms

$$r_n = \frac{c_n}{c_{n-1}} = \frac{1}{z_c} \left(1 + \frac{\gamma - 1}{n} + o\left(\frac{1}{n}\right) \right). \quad (\text{A.1})$$

It is then natural to plot the successive ratios r_n against $1/n$. If the correction terms $o(\frac{1}{n})$ can be ignored[‡], such a plot will be linear, with gradient $\frac{\gamma-1}{z_c}$, and intercept $\mu = 1/z_c$ at $1/n = 0$.

Linear intercepts l_n eliminate the $O(\frac{1}{n})$ term in eqn. (A.1), so in the case of a pure power-law singularity, one has

$$l_n := nr_n - (n-1)r_{n-1} = \mu \left(1 + \frac{c}{n^2} + O\left(\frac{1}{n^3}\right) \right).$$

Various refinements of the method can be readily derived. If the critical point is known exactly, it follows from eqn. (A.1) that estimators of the exponent γ are given by

$$\gamma_n := n(z_c \cdot r_n - 1) + 1 = \gamma + o(1).$$

If the critical point is not known exactly, one can still estimate the exponent γ . From eqn. (A.1) it follows that

$$\delta_n := 1 + n^2 \left(1 - \frac{r_n}{r_{n-1}} \right) = \gamma + o(1). \quad (\text{A.2})$$

Similarly, if the exponent γ is known, estimators of the growth constant μ are given by

$$\mu_n = \frac{nr_n}{n + \gamma - 1} = \mu + o(1/n).$$

Appendix B. Differential approximants

The generating functions of some problems in enumerative combinatorics are sometimes algebraic, such as that for $Av(1342)$ pattern-avoiding permutations, sometimes D-finite, such as with $Av(12345)$ pattern-avoiding permutations, sometimes differentially algebraic, and sometimes transcendently transcendental. The not infrequent occurrence of D-finite solutions was the origin of the method of *differential approximants*, a very successful method of series analysis for analysing power-law singularities [18].

[‡] For a purely algebraic singularity eqn. (7), with no confluent terms, the correction term will be $O(\frac{1}{n^2})$.

The basic idea is to approximate a generating function $F(z)$ by solutions of differential equations with polynomial coefficients. That is to say, by D-finite ODEs. The singular behaviour of such ODEs is well documented (see e.g. [19, 20]), and the singular points and exponents are readily calculated from the ODE.

The key point for series analysis is that even if *globally* the function is not describable by a solution of such a linear ODE (as is frequently the case) one expects that *locally*, in the vicinity of the (physical) critical points, the generating function is still well-approximated by a solution of a linear ODE, when the singularity is a generic power law (7).

An M^{th} -order differential approximant (DA) to a function $F(z)$ is formed by matching the coefficients in the polynomials $Q_k(z)$ and $P(z)$ of degree N_k and K , respectively, so that the formal solution of the M^{th} -order inhomogeneous ordinary differential equation

$$\sum_{k=0}^M Q_k(z) \left(z \frac{d}{dz} \right)^k \tilde{F}(z) = P(z) \quad (\text{B.1})$$

agrees with the first $N = K + \sum_k (N_k + 1)$ series coefficients of $F(z)$.

Constructing such ODEs only involves solving systems of linear equations. The function $\tilde{F}(z)$ thus agrees with the power series expansion of the (generally unknown) function $F(z)$ up to the first N series expansion coefficients. We normalise the DA by setting $Q_M(0) = 1$, thus leaving us with N rather than $N + 1$ unknown coefficients to find. The choice of the differential operator $z \frac{d}{dz}$ in (B.1) forces the origin to be a regular singular point. The reason for this choice is that most lattice models with holonomic solutions, for example, the free-energy of the two-dimensional Ising model, possess this property. However this is not an essential choice.

From the theory of ODEs, the singularities of $\tilde{F}(z)$ are approximated by zeros z_i , $i = 1, \dots, N_M$ of $Q_M(z)$, and the associated critical exponents γ_i are estimated from the indicial equation. If there is only a single root at z_i this is just

$$\gamma_i = M - 1 - \frac{Q_{M-1}(z_i)}{z_i Q'_M(z_i)}. \quad (\text{B.2})$$

Estimates of the critical amplitude C are rather more difficult to make, involving the integration of the differential approximant. For that reason the simple ratio method approach to estimating critical amplitudes is often used, whenever possible taking into account higher-order asymptotic terms [21].

Details as to which approximants should be used and how the estimates from many approximants are averaged to give a single estimate are given in [21]. Examples of the application of the method can be found in [22]. In that work, and in this, we reject so-called *defective* approximants, typically those that have a spurious singularity closer to the origin than the radius of convergence as estimated from the bulk of the approximants. Another method sometimes used is to reject outlying approximants, as judged from a histogram of the location of the critical point (i.e. the radius of convergence) given by the DAs. It is usually the case that such distributions are bell-shaped and rather

symmetrical, so rejecting approximants beyond two or three standard deviations is a fairly natural thing to do.

Appendix B.1. Biased differential approximants

If the critical point z_c is known exactly (or very accurately) one may try to obtain improved numerical estimates for the exponents by forcing the differential equation (B.1) to have a singular point at z_c , that is one may look at *biased differential approximants*. In [23] we developed a new method in which we form biased approximants by multiplying the derivatives in (B.1) by appropriate “biasing polynomials”. This allows us to bias in such a manner that the singularity at z_c is of order $q \leq K$. Let

$$F_k(z) = \left(z \frac{d}{dz} \right)^k F(z) \quad \text{and} \quad G_k(z) = (1 - z/z_c)^{q_k} F_k(z), \quad (\text{B.3})$$

where $q_k = \max(q + k - M, 0)$. With this definition we have that $G_k = (1 - z/z_c)^{q_k} F_k(z)$, while subsequent lower order derivatives have “biasing polynomials” of degree decreasing in steps of 1 (until 0). Then we form biased differential approximants (BDA) such that

$$P(z) + \sum_{k=0}^M \widehat{Q}_k(z) G_k(z) = O(z^{N+1}). \quad (\text{B.4})$$

For biased approximants the degree of the polynomial multiplying the k 'th derivative still have degree N_k such that the degrees of $\widehat{Q}_k(x) = N_k - q_k$ and the number of unknown coefficients is $\widehat{N} = K + 1 + \sum_k (N_k - q_k + 1)$.

Appendix C. Coefficient prediction

In [16] we showed that the ratio method and the method of differential approximants work serendipitously together in many cases, even when one has stretched exponential behaviour, in which case neither method works particularly well in unmodified form.

To be more precise, the method of differential approximants (DAs) produces ODEs which, by construction, have solutions whose series expansions agree term by term with the known coefficients used in their construction. Clearly, such ODEs implicitly define *all* coefficients in the generating function, but if N terms are used in the construction of the ODE, all terms of order z^N and beyond will be approximate, unless the exact ODE is discovered, in which case the problem is solved, without recourse to approximate methods.

It is useful to construct a number of DAs that use all available coefficients, and then use these to predict subsequent coefficients. Not surprisingly, if this is done for a large number of approximants, it is found that the predicted coefficients of the term of order z^n , where $n > N$, agree for the first $k(n)$ digits, where k is a decreasing function of n . We take as the predicted coefficients the mean of those produced by the various DAs, with outliers excluded, and as a measure of accuracy we take the number of digits for

which the predicted coefficients agree, or the standard deviation. These two measures of uncertainty are usually in reasonable agreement.

Now it makes no logical sense to use the approximate coefficients as input to the method of differential approximants, as we have used the DAs to obtain these coefficients. However there is no logical objection to using the (*approximate*) predicted coefficients as input to the ratio method. Indeed, as the ratio method, in its most primitive form, looks at a graphical plot of the ratios, an accuracy of 1 part in 10^4 or 10^5 is sufficient, as errors of this magnitude are graphically unobservable.

Recall that, in the ratio method one looks at *ratios* of successive coefficients. We find that the ratios of the approximate coefficients are predicted with even greater precision than the coefficients themselves by the method of DAs. That is to say, while a particular coefficient and its successor might be predicted with an accuracy of 1 part in 10^p for some value of p , the *ratio* of these successive coefficients is frequently predicted with significantly greater accuracy (the precision being typically improved by a factor varying between 2 and 20).

The DAs use all the information in the coefficients, and are sensitive to even quite small errors in the coefficients. As an example, in a recent study of some self-avoiding walk series, an error was detected in the eighteenth significant digit in a new coefficient, as the DAs were much better converged without the last, new, coefficient§. The DAs also require high numerical precision in their calculation. In favourable circumstances, they can give remarkably precise estimates of critical points and critical exponents, by which we mean up to or even beyond 20 significant digits in some cases. Surprisingly perhaps, this can be the case even when the underlying ODE is not D-finite. Of course, the singularity must be of the assumed power-law form.

Ratio methods, and direct fitting methods, by contrast are much more robust. The sort of small error that affects the convergence of DAs would not affect the behaviour of the ratios, or their extrapolants, and would thus be invisible to them. As a consequence, approximate coefficients are just as good as the correct coefficients in such applications, provided they are accurate enough. We re-emphasise that, in the generic situation (7), ratio type methods will rarely give the level of precision in estimating critical parameters that DAs can give. By contrast, the behaviour of ratios can more clearly reveal features of the asymptotics, such as the fact that a singularity is not of power-law type. This is revealed, for example, by curvature of the ratio plots [22].

As an example, consider the OGF for $Av(12453)$ PAPs (see OEIS [5] A116485). This is known to order x^{38} . Let us take the coefficients to order x^{16} and use the method of series extension described above to predict the next 22 ratios, so that we can compare them to the exact ratios. The results, based on 3rd order differential approximants, are

§ Given 69 terms of the square-lattice self-avoiding walk series, the 70th term is predicted by 4th order ODEs to be $4190893020903935057 \times 10^{12}$. The actual coefficient is $4190893020903935054619120005916$, which differs in the nineteenth digit. An error in the eighteenth digit was thus discovered during development. Several other less dramatic examples are known where lower-order errors have been discovered by this means.

shown in Table C1. For the first predicted ratio, r_{18} , the discrepancy is in the 10th significant digit. For the last predicted ratio, r_{39} , the error is in the 5th significant digit. This level of precision is perfectly adequate for ratio analysis.

Table C1: Ratios r_{18} to r_{39} actual and predicted from the coefficients of $Av(12453)$, with percentage error shown.

Predicted ratios	Actual ratios	Percentage error
10.654655347	10.65465504	4.78×10^{-7}
10.828226522	10.82822539	1.04×10^{-5}
10.986854456	10.98685140	2.79×10^{-5}
11.132386843	11.13238007	4.78×10^{-5}
11.266382111	11.26636895	6.08×10^{-5}
11.390163118	11.39013998	2.03×10^{-4}
11.504857930	11.50482182	3.14×10^{-4}
11.611441483	11.61138359	4.99×10^{-4}
11.710743155	11.71066190	6.94×10^{-4}
11.803496856	11.80338255	9.68×10^{-4}
11.890333733	11.89017822	1.31×10^{-3}
12.048402545	12.04814337	2.15×10^{-3}
12.120553112	12.12022972	2.67×10^{-3}
12.188650126	12.18824275	3.34×10^{-3}
12.252994715	12.25252103	3.87×10^{-3}
12.313939194	12.31336663	4.65×10^{-3}
12.371707700	12.37104982	5.32×10^{-3}
12.426619450	12.42581319	6.49×10^{-3}
12.478784843	12.47787509	7.29×10^{-3}
12.528486946	12.52743256	8.41×10^{-3}

In practice we find that the more exact terms we know, the greater is the number of predicted terms, or ratios that can be predicted.

Appendix D. Enumeration data

L	$C_L(1)$
1	8
2	95
3	2320
4	154259
5	30549774
6	17777600753
7	30283708455564
8	152480475641255213
9	2287842813828061810244
10	102744826737618542833764649
11	13848270995235582268846758977770
12	5613766870113075134552249300590982081
13	6856324633418315229580098999727214234534626
14	25264653780547704599613926971040640439380254497299
15	281194924965510769640501069703642937039678809002355743600
16	9461739046646537749639494171503923182753987897972167546351180871
17	963236702020101408274810653629921860636656580683490560257709270360444788
18	296872411379358777499142156584947972393781613934413706389772635139720532797697401
19	277150300263332125727926989254635730407844207233646123561354535935393720183262709640734296
20	784096265647396811778105941874438158236581845146768685766318151014460448963606598066808194055196391
21	6725180841063080568765785521839331530600623203136984200976765831832263641839818443238635675098039099764477094
22	174931600296771588816418921915331826961754552793606147578780164414287627531728146738237058492693139833462228085357900931
23	13803603811254425104633152972993523761617439474917134222103400574517678544806707098426335287312812055811653812588064999045835964788
24	330514809530329670032014436868916242065330006202515254218029114864900324594717492699469036772928641130210225812040363529280982602180021971501
25	2401952907672357993462515287034263569296810854353779576930606173996736217445824082165189903808422564905380792093559726262352646493540668423785540986958618
26	5299107129769378506953456534389910056797761651575284727185718491325361350700020349029824701741232397885203596081145956599662000200438618578333326328843424545244470913

Table D1: Number of SAWs spanning a square.

L	$P_L(1)$
1	1
2	3
3	42
4	1799
5	232094
6	92617031
7	115156685746
8	442641690778179
9	5224287477491915786
10	188825256606226776728029
11	20879416139356164466643759334
12	7057757437924198729598570424130207
13	7287699030020917172151307665469211016474
14	22973720258279267139936821063450448822110219653
15	220999541336018343231658363621596453585823579325485544
16	6485093759718494344865537501691711476194821918864090506157759
17	580338710138214792049192419944468721379579881619954352303395183377868
18	158337812302865122325340454524668159260049140429114314750279637797162731935795
19	13168613394347732349631997498349027181530263294062454367517883251973010678492927145164
20	333791921301450408656424393731824932225524914478794139217214328043764176667483451057387588939581
21	2578284699331238205287505462049410591202075986811965490195831413301513664200106021200647983846671319023376
22	60681018617202345518945611945550350166677922700280807250098751378055134432090527432691244436095874301999620318286417
23	4351075330271556361458913058062785859178198294438374222572342619944855786600569691060003274678918267681800765492921507255444030
24	950435810029045769123624069823361419361696021093908583594503116871962553684187067543456237120685036487281955076387155649492347583783912357
25	632407534045235304278897181408229137621456170029071955419475667299649868819055002950538251352503131227737994021488874040396259243064748293794055487122
26	1281707896370751708653066922805265028882836851074044433082078379196572742914435468007626647333767206265847516495713522985546806840650483671342846200191630108286969

Table D2: Number of SAPs crossing a square.

L	$C_L(1)$
1	2
2	14
3	316
4	25092
5	7374480
6	8029311942
7	32223151155864
8	476605408516689238
9	26016526700583361056456
10	5246595079903462547245876694
11	3911053741699230141571030313824664
12	10780907768757190963361134040036893772360
13	109919900687141309301630828947780890728732496678
14	4146148169372563020871034877194447551275644544417216784
15	578668580332775727107695799371628560927178835729875790606922120
16	298872860145313265329322304090348192097227121631333193254451061450023212
17	571292892753639610811496925540653319819009464854621261888736201676638277892860364
18	4041877636548925601268934261053439777968614414770138847482643177563162891499826990868686710
19	105849680445660298017662516167192274494877530131095615720184731073055676134641221548956561836515847160
20	10261319175888813072109344281334022257660847729142398797395911985785352481803270582806576593011349057648597629702
21	3682522861496742274013714098245794929775776187625314598131060860173699707921073898860823021154156312609385314847082364604336
22	4892542075116215747349775890169094456449789602921450060431267745393588411359934920766964621175270271453676206611892541512628195569791000
23	2406502263599131862433203790219664413324113905029856267315583453701973757695375525767612997770681689706285684286956275152985138134931365323467344612
24	438242218832195088801894111132005025739819100831104898458347287148981323073167259406443353675374485580614409526121217079214285336977046690201810752933696772629332
25	29548150764354051108986653372266838516881491330935777859166128849296753863671730114976395779815333178178360613565695537261400270819437732521145740229031786418466822328155210774
26	7376409612724881246275082273655527171437045694901336339786650436361148933382241819470915896534342159863922343241461009706359183544468912989538551447112728993641722959010706705865911047130282

Table D3: Number of SAWs crossing a rhomboidal domain of the hexagonal lattice.

L	$C_L(1)$
1	2
2	50
3	2256
4	292006
5	124394172
6	182189852062
7	937116505296162
8	17167376550995687961
9	1130911800993488803731078
10	269650395624478266477331223678
11	233772496350603982679550385266064014
12	739330863241806743025423160490836132227125
13	8551000409049037000098287028025432585191736309022
14	362378501157171575915086740862352731989136965188978227480
15	56355164888855923540517493455292977980691264400637162090248666536
16	32200232301152973892060847293393239105831802930525492217459523426803019578
17	67665662468515970834966508500944029204762050650693102413477819738278462353187499568
18	523379303813002076273464810690096008845689319359263297454993915567005968614237413818526075604
19	14910759530495548949623554019916848509888902630562528597658761833271654794704911307455162596911430188758
20	156552766529028680644951163416182891619237381422347104413735417263587336683056846547108571311383043144417391243521
21	606084065190103550545340197138093542241444175895240820944713102199472484407589836051473378294437969118344993099132112988392420
22	865520866516174852434302085316123704413013184383267585803777199791333436065070398518809805939514793360791184628285127191002600593996365368
23	4560992075553129850922927762995312993575376533697147813417446333497150777368818523814441027249715528879466279022480571252085818753070411144055018204876
24	88718729299059562850997307819335993122314801341423818394843508516540284335394844383553598429174621313143090882997603769027577322213964104279601294505719147199388248
25	6371850587510704465849294714166605694358498327959158268953676175064720102088107446652503452424238514332661839511396033679344990952004170416492446601538481306356885482155377886638
26	169011336127263808956441260014789508545122612515869787545534380630798876325920139245100711076793585499650454967955439732124691809189880222542458839160812960021404785245887985513225511176452673

Table D4: Number of SAWs spanning a rhomboidal domain of the hexagonal lattice.

L	$P_L(1)$
1	1
2	3
3	48
4	3126
5	775842
6	727870836
7	2575728525240
8	34244061451559094
9	1703999058661009145746
10	316543880488539946466963896
11	219157996022284922702859434801868
12	564858713948847373563461482383973674774
13	5415142061627863782256892670635702203299498106
14	19296590885945525522444585453472066280402031983076676
15	25546198443752201604792021828520875111113011948793636471115986
16	12559327077982128401344048554297110314066721517873014754182697036556596
17	22922091883660814526614648049302957461020819783000936029058072227670397210344452
18	155263447483572551766390960410624837560693086531157173552843098568401053874449090345960952
19	3902210830303866544089288909268585128297599458763876386711662682968145520021314838767588755204876552
20	363826279944404033043481454750498594828384686156661907448081883116767989915064170563158680799058587038093669970
21	125819288614038800635491456373348096978155582443835316985068491781106711591018731348747689905774023677560616130526519792788
22	161364676308721043071062335667640391981582844992152210690103275445701605800992646736829901291623422443479273978505601685944958319502908
23	767404723000807383687986740560681434496809093061630495379302826095788965371427398181191526510671680461233928816145587981072980847709460390319231092
24	13531589671078110974893162463064998617986779218655081753249240837076015118491730281579616308320287573428293648926750890064755844067619542837352365219373425001182
25	884587740071585897410736339557658407744835896491278031519338391577738398470263456602417012949952825706708843546792281536393617902202119150298209236054002295717190761721586136
26	214370491395195888234645652662533040178049645573231037100079862232102374051311163431171231717044978758387398235068063926962934021314526635561030249606476912450218466192900542978818780384974

Table D5: Number of SAPs crossing a rhomboidal domain of the hexagonal lattice.

L	$C_L(1)$
1	2
2	7
3	44
4	515
5	11500
6	493704
7	40751496
8	6463642330
9	1970190022696
10	1154437344815284
11	1300686960810345198
12	2818300749120970598426
13	11745284697899678209887246
14	94153940687296424300453605522
15	1451915619132744566900848537333082
16	43072062058620235613855525243039798546
17	2458218787430131938141065342199631011888808
18	269917990612156037679955033913220231218482526540
19	57022048161016261704452967864058833682099233234074924
20	23177397882827812987656054354088621630193659021408496092114
21	18126208865601871898868235390674787298375068592505362074324218782
22	27275828087021466037231281803108531532614036012259410718518383677989994
23	78974101601865877096497572762267816542675600879070694217812459537275320667130
24	439980515324228439963646464930268543060978419686632840124513851873692354257184355418
25	4716606546189621488078969490297265985170243927748285792380749595975920915553704131199964610
26	97292222614020401528875654356525325735532995996523907301076613477132417329484579095044048258220716
27	3861740982967126791934974463996504445993431827647538470677158069324943832308988274731817887045190314942500

Table D6: Number of SAWs crossing a triangular domain of the hexagonal lattice.

L	$C_L(1)$
1	1
2	3
3	18
4	210
5	4716
6	203130
7	16781528
8	2661898722
9	811337884328
10	475395297020430
11	535618774376758222
12	1160567857061063474508
13	4836675324919658534327348
14	38772333263059858336182467950
15	597894854584620490267288203881970
16	17736956492510173648327596231133813426
17	1012287723222402775005385313973408357507928
18	111151484863070215708849728284201214059413569272
19	23481522343431693736560242087640111797935241906792060
20	9544388601505664173784379076794209212239937007395941459026
21	7464322880925069857683897811600948880215514557439627560911154272
22	11232110875321164747567467659828479928446150234247426811308149074039470
23	32521317511278850216940549112361104580618379635763819229016915699625133297104
24	181182764336015552734273130240200423605997687829676784582391379637383247087868602758
25	1942285584539983234933331010286728144642773519634047277599154248174196516886152824735901816
26	40064669298138196682088095071796367265068180648770697785528635200087726423296089992305061500566756

Table D7: Number of SAWs crossing a triangular domain of the hexagonal lattice and including the top vertex.

L	$P_L(1)$
1	1
2	2
3	9
4	85
5	1605
6	59896
7	4392639
8	629739138
9	175745776816
10	95207239875508
11	99934927799315359
12	202993550188918062298
13	797200289814680588454420
14	6048794511036987586252009778
15	88623124229469033988344357343229
16	2506168305598107863294101582119745559
17	136742066892485673488096591777101574684341
18	14391095306419863125025082539141317797920679808
19	2920637571762330449794165953013715565926946586966972
20	1142780121652579092442989213824129363529214905674607409456
21	861928813419640412952428304528142087056944927600343349249100770
22	1252960133060510490994725871202276919994651077934833437111933731780232
23	3509963453723621942826513300378279853247659026894598196945505524358307547596
24	18945984524072416973165104755335799616808372006565339168062614482119446796495592941
25	197032077332349626704638536077733550874900563736415557346148448949082140805149991012506724
26	3947507851539205775146388396017001015202508590957965919271768932077125446293950595857281240459716

Table D8: Number of SAPs crossing a triangular domain of the hexagonal lattice.

L	$P_L(1)$
1	1
2	1
3	4
4	36
5	666
6	24696
7	1808820
8	259300148
9	72369408510
10	39205936157880
11	41152969216872016
12	83592236529606631688
13	328284931491454739745904
14	2490876950205850778116435156
15	36494758452603010620499864088198
16	1032033208911845667821292289616451218
17	56310006747344597198073248186075772148180
18	5926213428826485611611313527823854932071080074
19	1202710510511720770819662867223620040669484274841448
20	470593707331440145848250079430318880733169905225241510182
21	354939911811827613400027738254513445185773676790950877558157556
22	515965532286678291640886325718842923532551840839177342378988626653078
23	1445393283922054883637378235832608861381031003585207142018132021675532043232
24	7801904249270681046277482881424254681239226301915609070185058428520166740304455480
25	81137266805100512823257637730776600977600011085064069900554442194897045916216667639237206
26	1625572861413431635691529107338978659074358348381654539274841326821635464880471185029440059346822

Table D9: Number of SAPs crossing a triangular domain of the hexagonal lattice and including top vertex.

L	$C_L(1)$
1	2
2	14
3	264
4	21512
5	5663596
6	6478476233
7	23432328776346
8	365121393771314359
9	18039965927005597824652
10	3847346539490622663060402802
11	2604549807872636495439504536518768
12	7613280873970130888072912524910312775000
13	70659728324509466176595292882340210105184200002
14	2831956810062815172946024396329723966506233510418891138
15	360424703055912928274223706157781269084968015495478379832577374
16	198097258016637755765939369950089310341388296845374445597477414443215248
17	345765524783138086318892247783650000160221384394056330912454668222835230637412672
18	260633888464918750654339908235496224103664480771353337217794306196421868029243067294778048
19	62392663751835087636515340004811611674555874089327041316405089409127243514061643853154930821350090724
20	6450407172867437933486941949195444800686042090585344770339862190617805415359568631117548255651795966774975729408
21	211788567928775963866338997256258041472352046409554241361185972450931528316998669866888918984500033887174419453417031840108
22	3003111631506205594200550519402977342109069309804916734448892038737633365710727044910318753595074453487711557977426845717574589858142229
23	13524071180124614895872809797043935746289243109268223573969721018213938124696255997302291968299972324147755286357424784253377182127831016598030435648
24	26302583800002506267728179467786825301378641433800017689615980657976366151408147401274046080321228727574309853794611789046332691442399607521892487626528327350411

Table D10: Number of SAWs crossing a square domain of the hexagonal lattice.

Appendix E. Supplementary numerical analysis

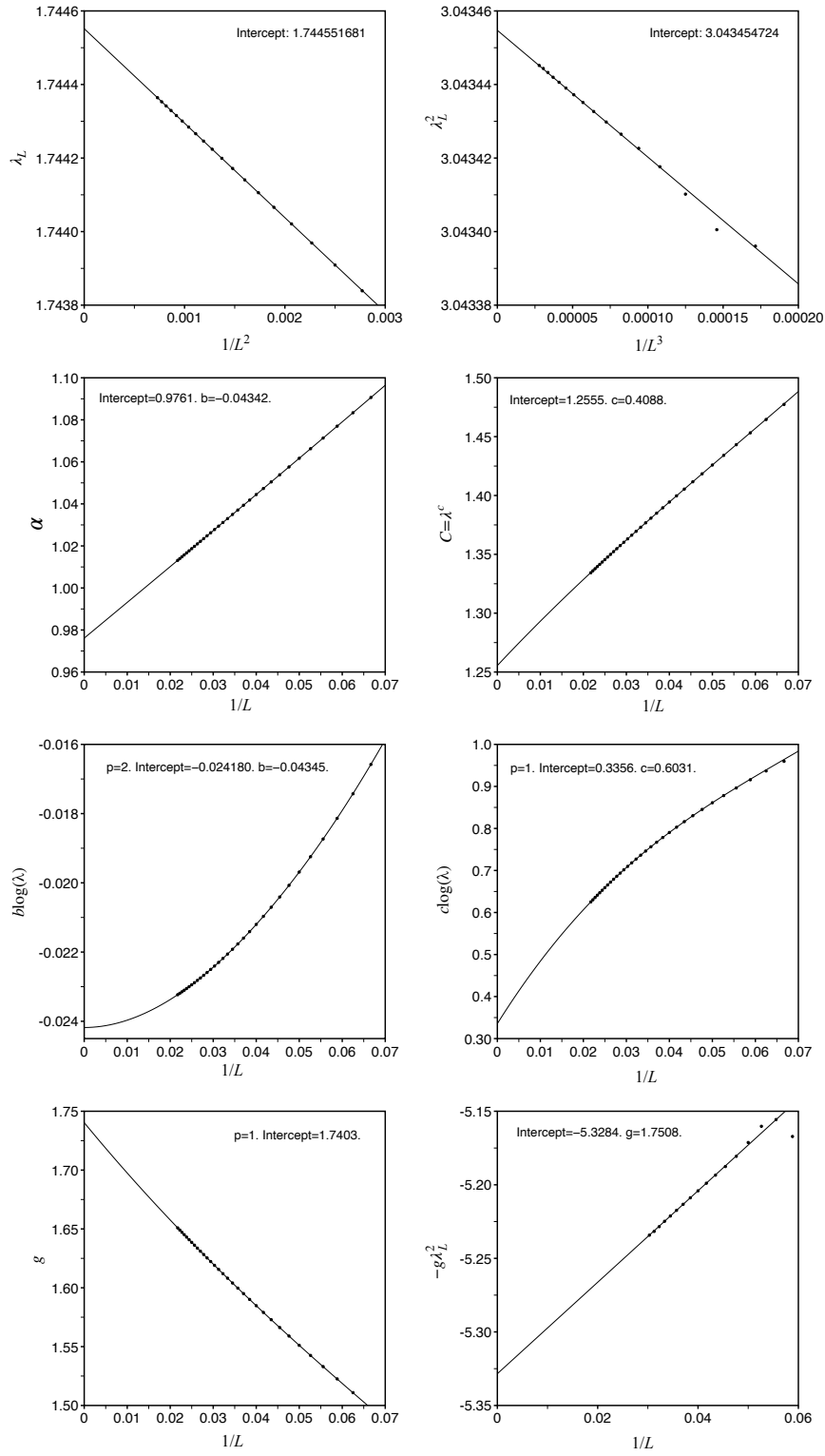


Figure E1: Plots of the various estimators used in the analysis of the data for SAWs spanning a square.

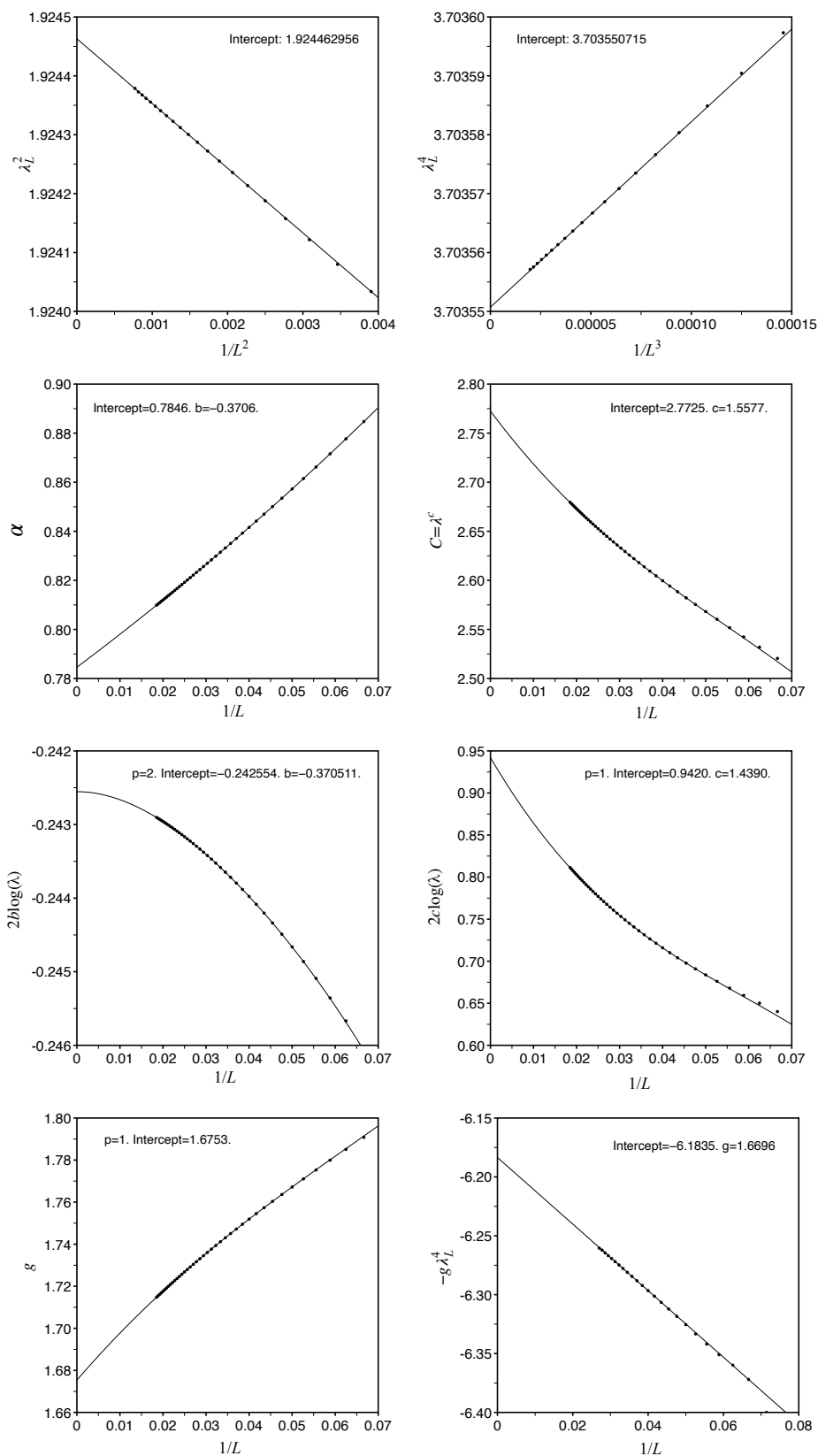


Figure E2: Plots of the various estimators used in the analysis of the data for SAWs spanning a rhomboidal domain of the hexagonal lattice.

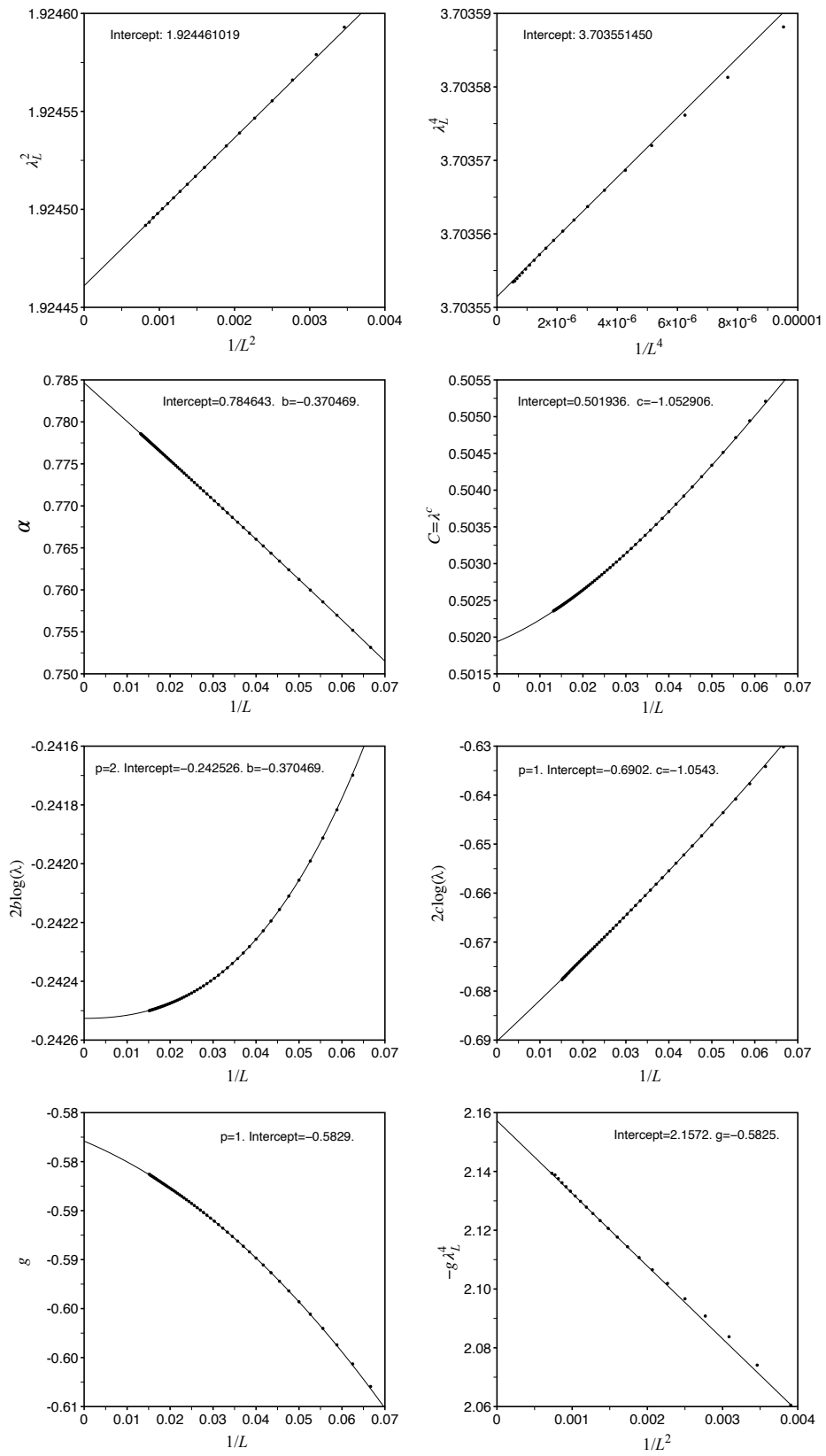


Figure E3: Plots of the various estimators used in the analysis of the data for SAPs crossing a rhomboidal domain of the hexagonal lattice.

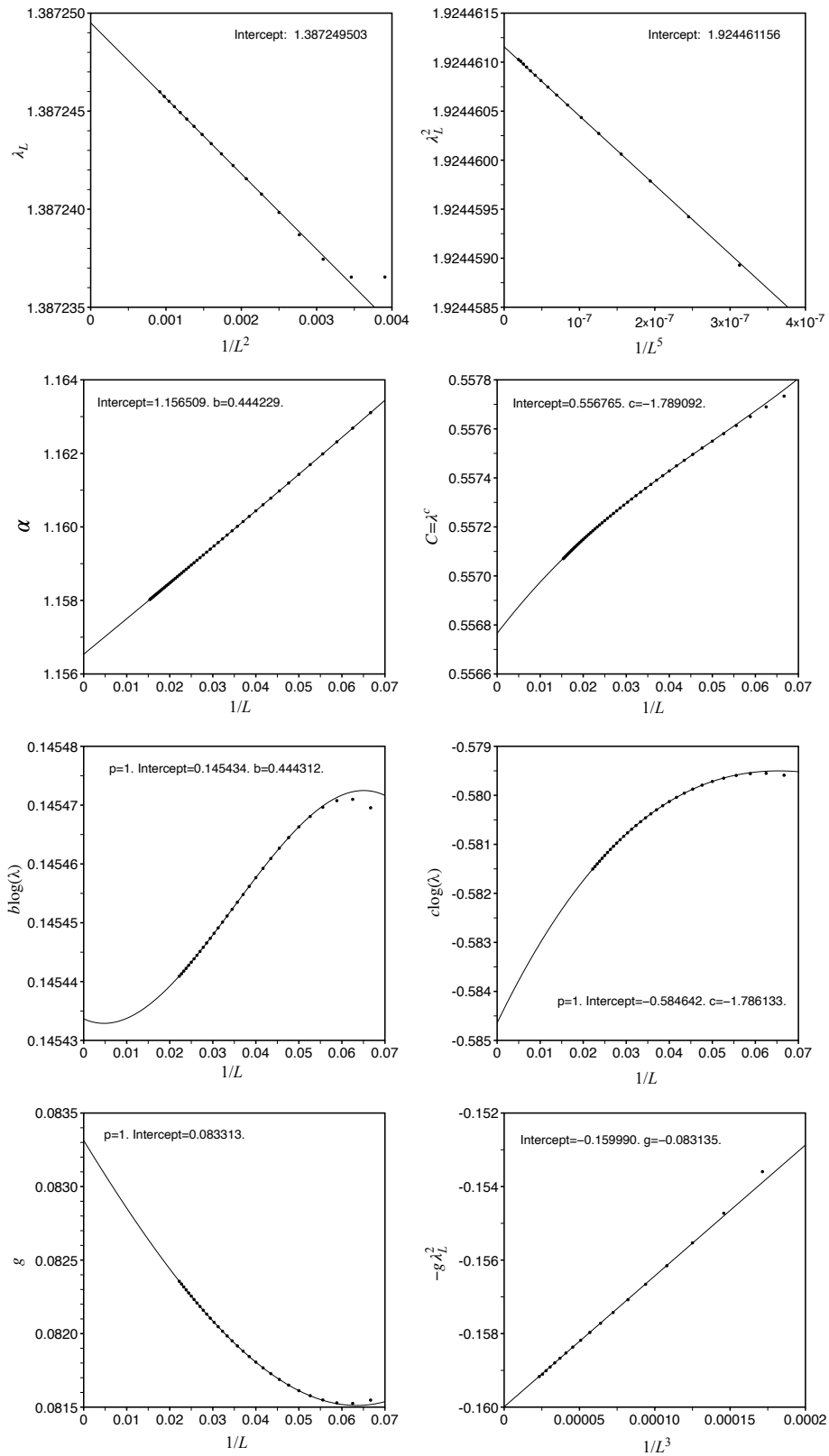


Figure E4: Plots of the various estimators used in the analysis of the data for SAWs crossing a triangular domain of the hexagonal lattice while passing through the topmost vertex.

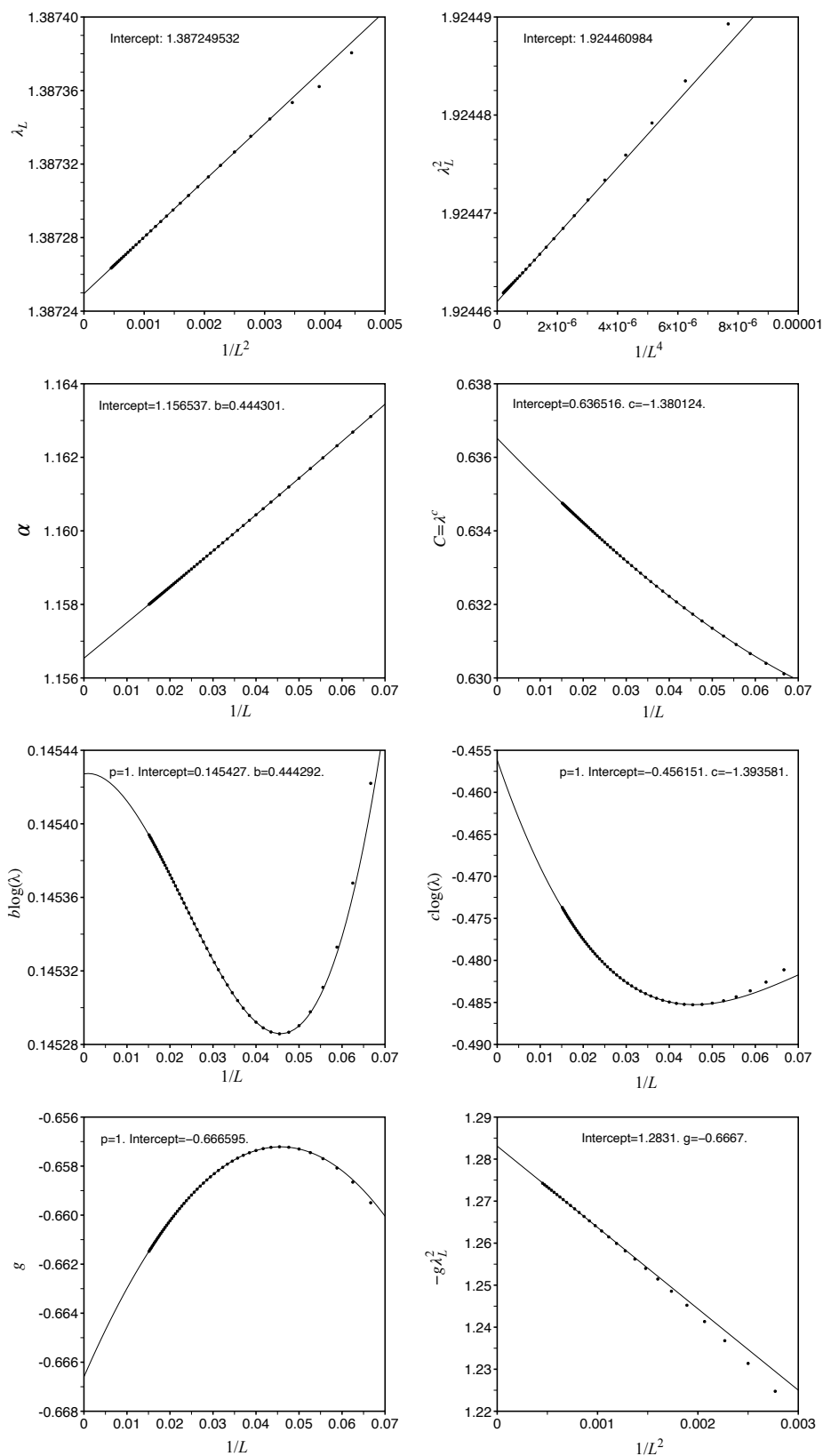


Figure E5: Plots of the various estimators used in the analysis of the data for SAPs crossing a triangular domain of the hexagonal lattice.

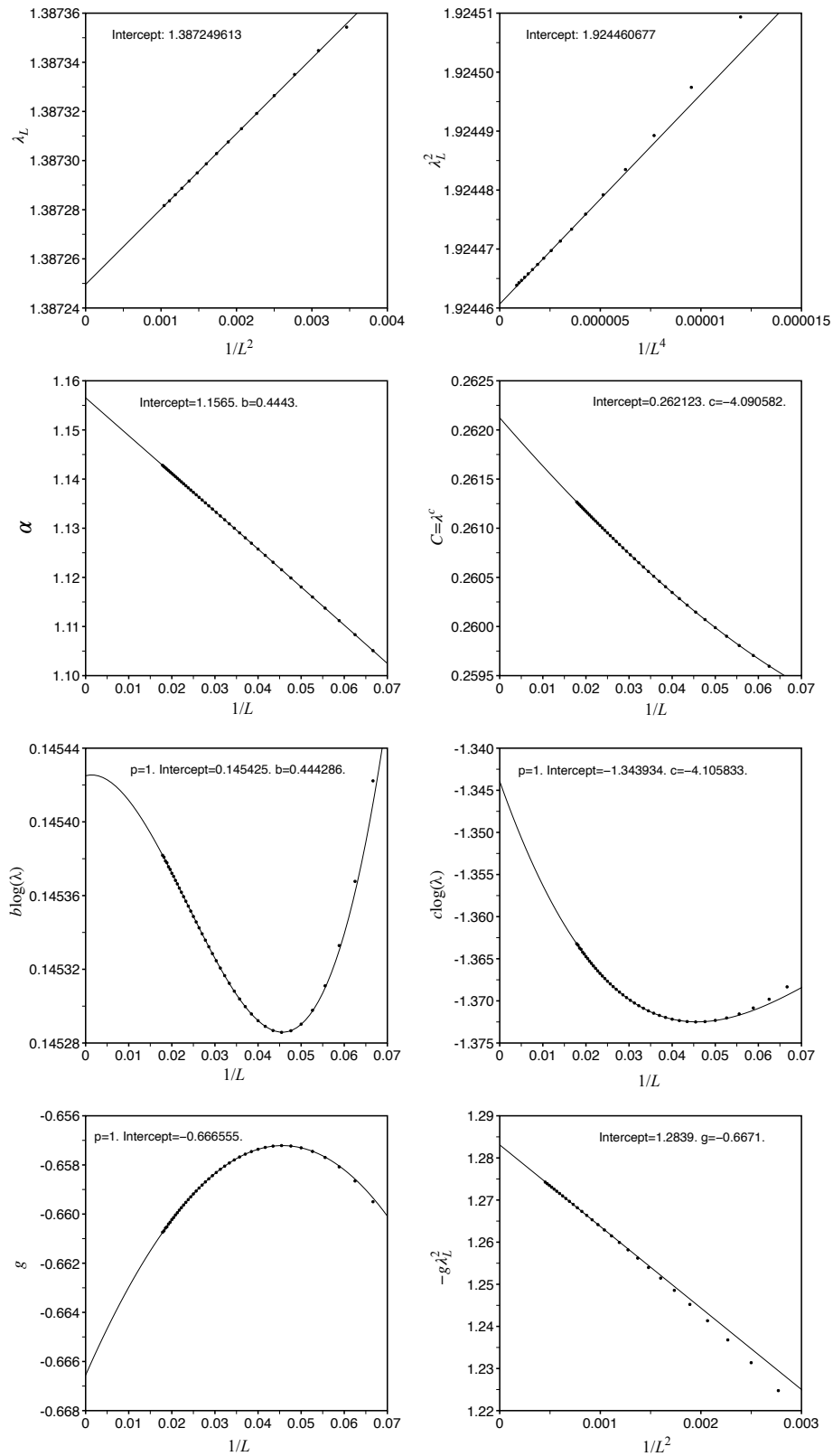


Figure E6: Plots of the various estimators used in the analysis of the data for SAPs crossing a triangular domain of the hexagonal lattice while passing through the topmost vertex.

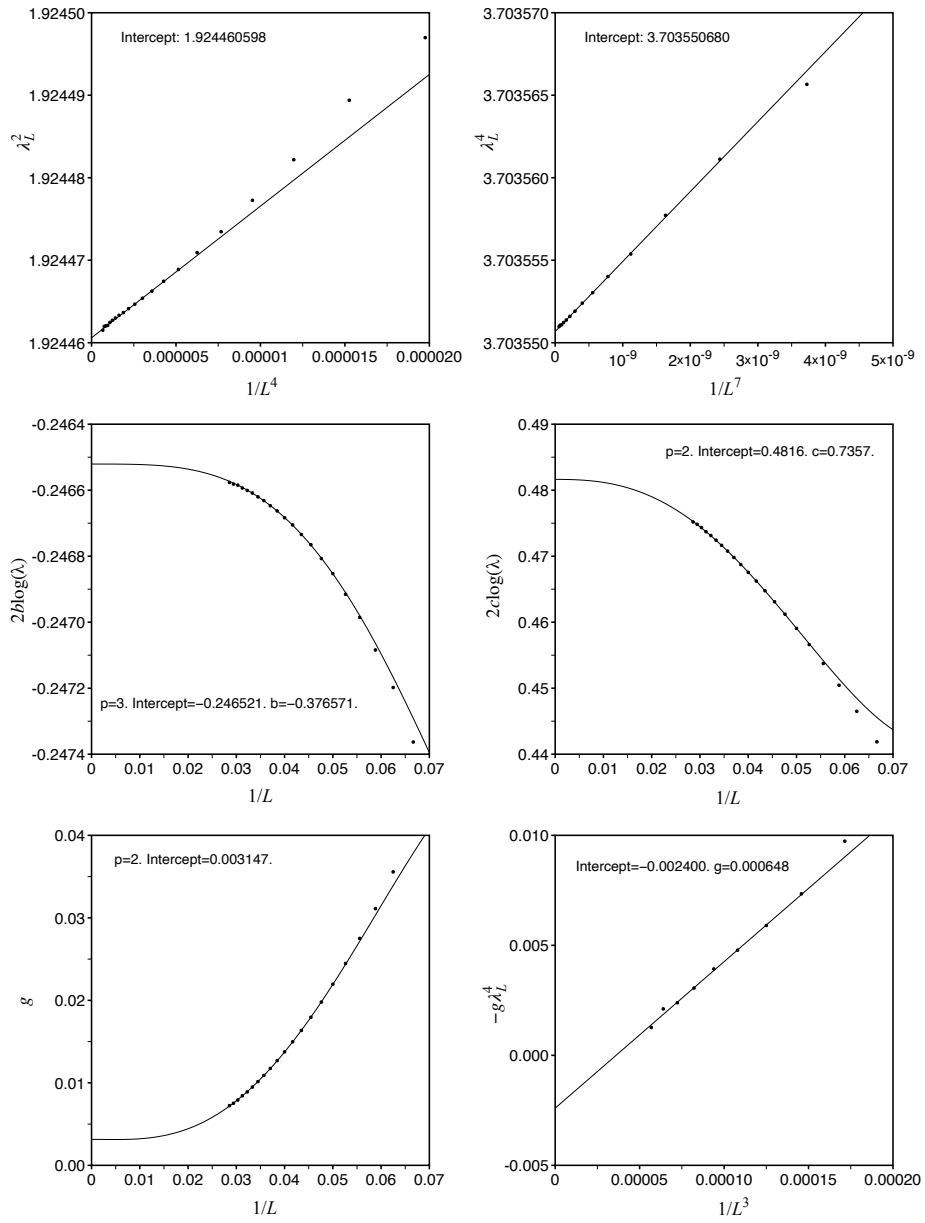


Figure E7: Plots of the various estimators used in the analysis of the data for SAWs crossing a square domain of the hexagonal lattice.